Computational Alchemy: The Rational Design of New Superhard Materials

David Michael Teter

Dissertation submitted to the Faculty of the
Virginia Polytechnic Institute and State University
in partial fulfillment of the requirements for the degree of

Doctor of Philosophy
in
Materials Engineering Science

Professor G.V. Gibbs, Co-Chair
Professor M.B. Boisen Jr., Co-Chair
Professor D.F. Cox
Professor W.A. Curtin
Dr. C.T. Prewitt

June 29, 1998
Blacksburg, Virginia

Keywords: Structure prediction, superhard materials, high-pressure

Computational Alchemy:
The Rational Design of New Superhard Materials

David Michael Teter

First–principles electronic structure calculations have been performed to help identify and direct the synthesis of new superhard compounds. An improved figure of merit for hardness is identified and used to show that carbon nitrides are not likely to be harder than diamond.

This work was supported by the following National Science Foundation grants: NSF-8920239, NSF-9303589, and NSF-9627458.

Dedication

I dedicate this dissertation to my daughter Elora and to my son Finley. Without them, this would never have happened. Thanks kids, I owe you.

Acknowledgements

First, I wish to deeply thank Jerry Gibbs, Monte Boisen and Charlie Prewitt for their support and encouragement, for setting high standards, and most importantly for being such wonderful people.

I'd like thank Dave Cox, Bill Curtin, Steve Kampe and Bill Reynolds for their good advice, their kindness and willingness to help and for the beer.

I thank the friends that I made in Blacksburg, Washington, D.C., and points elsewhere. Their friendship is one of the most important things that I have gained from this effort. Many thanks to: Heidi Allison, Mark Asta, Jimi Badro, Jennifer Blank, Pan Conrad, Bob Downs, James Farquhar, Dan Frost, Tahar Hammouda, Joel Ita, Ashraf Khan, Boris Kiefer, Stephanie Kitchel, Tom Kuhr, Joel Lee, Kevin Lithicum, Jud Marte, Ryan McCormack, Sesbastien Merkel, Greg Moore, Dane Morgan, Vidvuds Ozolins, Jay Senkevich, Maddury (Zulu) Somayazulu, Becky and Mike Stawovy, John Vandecar, Suzan van der Lee, Anne Villette, and Cecily Wolfe. Thanks especially to Mike Stawovy for being such a great friend.

I thank the fine scientists that I have had the pleasure of working with and learning much from: Doug Allan, Neil Ashcroft, Ben Burton, R.W. Cahn, Gerd Ceder, Bob DeVries, Bob Hazen, Rus Hemley and Georg Kresse.

I'd like to thank my father for setting high standards and and encouraging me following

them. Well, at least for setting such fine *professional* standards.....

And finally, I thank my wife Stuart for her love and for her support.

This work would not have been possible without the greatly appreciated support of the National Science Foundation.

Contents

1 The Rational Design of New Materials **1**

1.1 Introduction 1

1.2 Superhard Materials 2

1.2.1 Selecting Promising Chemical Systems 4

1.2.2 Generating a Set of Reasonable Crystal Structures 7

1.2.3 Selecting a Method for Calculating Energies 12

1.2.4 A Calculation of the Bulk Modulus 13

2 Determining a Better Figure of Merit for Predicting Hardness **16**

2.1 Introduction 16

2.2 Determining a Better Predictor of Hardness 18

3 Carbon Nitrides **28**

3.1 Introduction 28

3.2 Methodology 32

3.3 Results 33
3.4 Discussion 37
3.4.1 Energetics and Structure: The effect of lone-pair interactions 37
3.4.2 The Role of Pressure in the Synthesis of Carbon Nitride 42
3.4.3 Predicting the Hardness of Carbon Nitrides 44
3.5 Conclusions 49

4 High Pressure Phases of Silica **50**

4.1 Introduction 50
4.2 Computational Details 51
4.3 Generation of New Structure Types 52
4.4 Results and Discussion 53
4.4.1 Sequence of High Pressure Phase Transitions 53
4.4.2 A Rexamination of Recent Experimental Data 60
4.4.3 Predicting the Hardness of High–Pressure Phases of Silica 62
4.5 Conclusions 64

5 Conclusions **65**

5.1 Conclusions 65

6 Future Work **67**

7 Bibliography **68**

List of Figures

1.1 A suggested strategy for the rational design of new materials. 3

1.2 Hardness vs. bulk modulus for Group IV and Group III-V tetrahedral semiconductors. 5

1.3 Representations of the (a) high–cristobalite, (b) diamond, (c) high–tridymite and (d) lonsdaleite crystal structures. 10

1.4 Representations of the (a) $CaCl_2$ and (b) α–PbO_2 structure types of SiO_2. The left–hand figures show one layer of the $ABAB$... stacking of *hcp* oxygen anions (white) with one–half of the octahedral interstices filled with silicon ions (black). The right–hand figures show how these patterns form edge–sharing octahedral chains with various degrees of kinking. 11

1.5 Energy-volume curve for cubic–BN. 15

2.1 Comparison of hardness with the bulk moduli for a wide variety of hard oxides, nitrides, borides and carbides. 21

2.2 Comparison of the hardness with the shear moduli for a wide variety of hard oxides, nitrides, borides and carbides. 22

2.3 Comparison of the hardness with the Young's elastic moduli for a wide variety of hard oxides, nitrides, borides and carbides. 23

2.4 Comparison of the Young's elastic moduli with the shear moduli for a wide variety of hard oxides, nitrides, borides and carbides. 24

2.5 Comparison of the hardness with the atomic density for a wide variety of hard oxides, nitrides, borides and carbides. 25

2.6 Comparison of the hardness with the cohesive energy density for a wide variety of hard oxides, nitrides, borides and carbides. 26

2.7 Comparison of the hardness with the band gap for a wide variety of hard oxides, nitrides, borides and carbides. 27

3.1 Representations of the (a) α–C_3N_4, (b) β–C_3N_4, (c) defect–zincblende-C_3N_4, (d) cubic–C_3N_4 crystal structures and (g) a single layer of graphitic C_3N_4. . 31

3.2 Cohesive energy vs. unit cell volume for several polymorphs of C_3N_4. 36

3.3 Total electronic density of states for several of the carbon nitride polymorphs discussed in the text. 40

3.4 Representation of the C_4N_3 structure described in the text. The dark atoms represent the carbon atoms, while the light atoms represent the nitrogen atoms. 41

3.5 ΔH of various carbon nitrides vs. pressure 43

4.1 Representations of the (1a) $CaCl_2$, (1b) 4X4–SnO_2, (1c) 3X3–$NaTiF_4$, (1d) 3X2 $P2_1/c$, and (1e) α–PbO_2 structure types. The left–hand figures show one layer of the $ABAB...$ stacking of *hcp* oxygen anions (white) with one–half of the octahedral interstices filled with silicon ions (black). The right–hand figures show how these patterns form edge–sharing octahedral chains with various degrees of kinking. 57

4.2 Enthalpies of silica structures relative to the enthalpy of stishovite as a function of pressure. 58

4.3 Representations of the high–pressure $Pa3$–SiO_2 structure in terms of a ball and stick and a polyhedral models. 59

List of Tables

1.1 Bond lengths and bond stretching force constants for some chemical bonds between first and second row atoms. 6

1.2 Two– and three–component systems isoelectronic with diamond recommended by Zhogolev *et al.* for the synthesis of new superhard materials. 8

1.3 Comparison of theoretical and experimental cubic–BN bulk moduli 14

3.1 Calculated structural zero–pressure structural parameters for the carbon nitride structures discussed in the text. 30

3.2 Calculated structural zero–pressure structural parameters for the carbon nitride structures discussed in the text. 39

3.3 Results of LDA calculations to determine the (c_{11}-c_{12}) shear modulus of cubic–C_3N_4 using a [444] MP–grid at a kinetic energy cutoff of 347.853 eV. 48

3.4 Results of LDA calculations to determine the c_{44} shear modulus of cubic–C_3N_4 using a [444] MP–grid at a kinetic energy cutoff of 347.853 eV. 48

3.5 Bulk and shear moduli for several of the carbon nitrides considered. 48

4.1 Calculated zero–pressure structural parameters for the structures described in the text. 56

4.2 Comparison of Kingma *et al.* diffraction data to the theoretical diffraction record of the $P2_1/c$–type at a pressure of 173 GPa. 61

Chapter 1

The Rational Design of New Materials

1.1 Introduction

A pressing challenge facing modern materials science today is the rational design and synthesis of new materials possessing exceptional properties.[18, 19, 28, 24, 25, 27] This has become an achievable goal due to recent advances in first–principles modeling methods[158] and the availability of increasingly affordable and powerful computational resources. The strength of these methods lies in their predictive abilities; they are not only able to reproduce the crystal structures, bulk moduli and elastic properties of a large class of materials to within 2-3% of the experimental values, but they have also been successful in the prediction of a number of phase transitions that have been verified experimentally.[94]

Despite the power of these methods, the process of designing materials from first–principles is usually not a straightforward or simple task. It requires overcoming a number of obstacles, some of which are quite formidable. First, a calculable figure of merit that correlates well with the desired property must be established. For example, the well known connection

established between the hardness of a material and its zero pressure modulus (K_0) is an example where a calculable quantity, the bulk modulus (a measure of resistance to volume change upon reversible hydrostatic compression), can be used as a figure of merit for hardness, the greater the bulk modulus, the harder the material. While the establishment of a figure of merit may be straightforward in some cases, in others the process of reducing a complex property to a single calculable variable can be rather difficult. Next, a promising chemical system and a viable set of crystal structures must be determined. This is not a trivial task as the prediction of structures that can crystallize in a given system can be an exceedingly challenging task. Next, a strategy for calculating the energies and the figure of merit of the desired property of the structure must be established. The steps followed in proposing a figure of merit and using it to design and discover a material with a desired physical property are in Figure /refmethod.

1.2 Superhard Materials

An exciting example of the process of designing materials from first principles is the on–going search[4, 15, 37, 38, 42, 108, 111, 112, 113, 114, 128, 167, 168, 173, 186, 189] for new superhard materials. Several hundred experimental efforts to synthesize and characterize such materials have been launched based upon the premise that the hardness of a material is closely related to its zero pressure bulk modulus (K_0), the greater the bulk modulus, the harder the material. [26, 53, 110, 116, 163, 189, 229] As is well known, diamond is not only one of the hardest materials known (superhard), but it is also one of the most incompressible materials. Superhard materials are defined as materials having a Vickers microhardness exceeding 40 GPa.[189] In addition to great hardness, superhard materials usually possess other unique properties such as high thermal conductivity and compressional strength. This

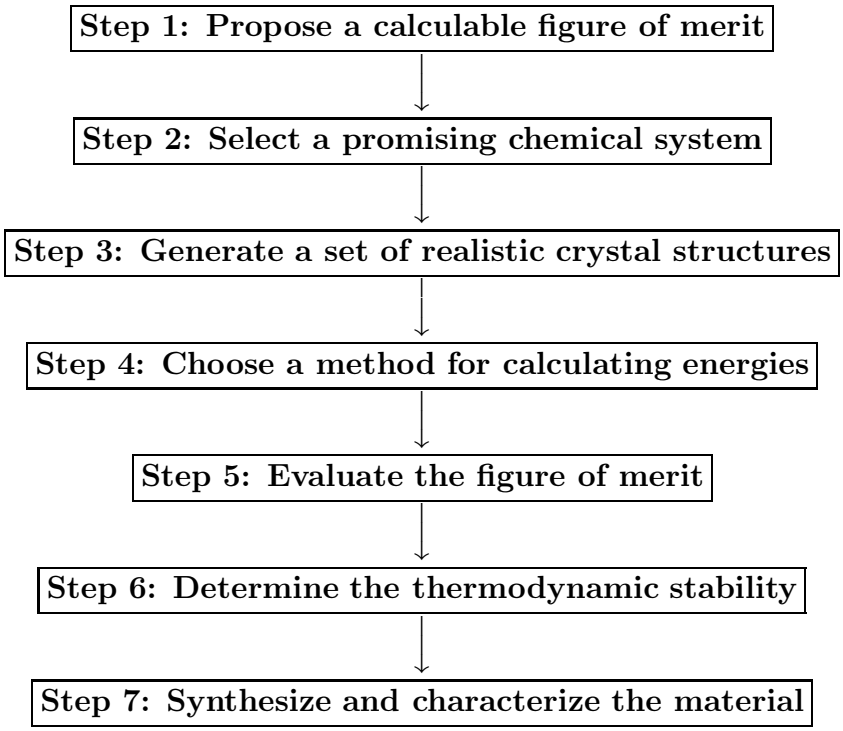

Figure 1.1: A suggested strategy for the rational design of new materials.

combination of properties makes such materials highly valuable in industrial applications such as superabrasives, wear resistant coatings, heat sinks, radiation windows and even surgical knives. Indeed, superabrasives have an annual consumption currently approaching 200 tons with an approximate value in excess of 1 billion U.S. dollars.[189]

In this section, we will examine a strategy for searching for materials that are potentially superhard and alternative procedures for formulating a recipe for their synthesis. Recently, several hundred experimental efforts to synthesize and study new superhard materials have been initiated based upon theoretical predictions that certain carbon nitrides have a K_0 value approaching[23, 116, 118, 119, 154, 166, 197, 230] and even exceeding[197] that of diamond.[26, 53, 110, 116, 163, 189, 229] As displayed in Figure 1.2, the strong correlation between hardness and K_0 shows that this relationship applies well to the Group–IV and Group III-V tetrahedral semiconductors with the hardness of these materials tending to increase linearly with K_0.

1.2.1 Selecting Promising Chemical Systems

As observed above, diamond is one of the hardest materials known to man. It possesses a Vickers hardness of approximately 100 GPa. It also has the highest bulk modulus (443 GPa) known for any material. [54] In the search for other hard materials, it seems worthwhile to consider the properties of other possible materials with the diamond structure that possess strong homodesmic chemical bonds. For any material like diamond whose volume can be uniquely described in terms of the bond length, K_0 can be related to the quadratic–bond–stretching force–constant (f_c(MX)) and the equilibrium bond length (R(MX)). The relationship between these variables is given by the expression

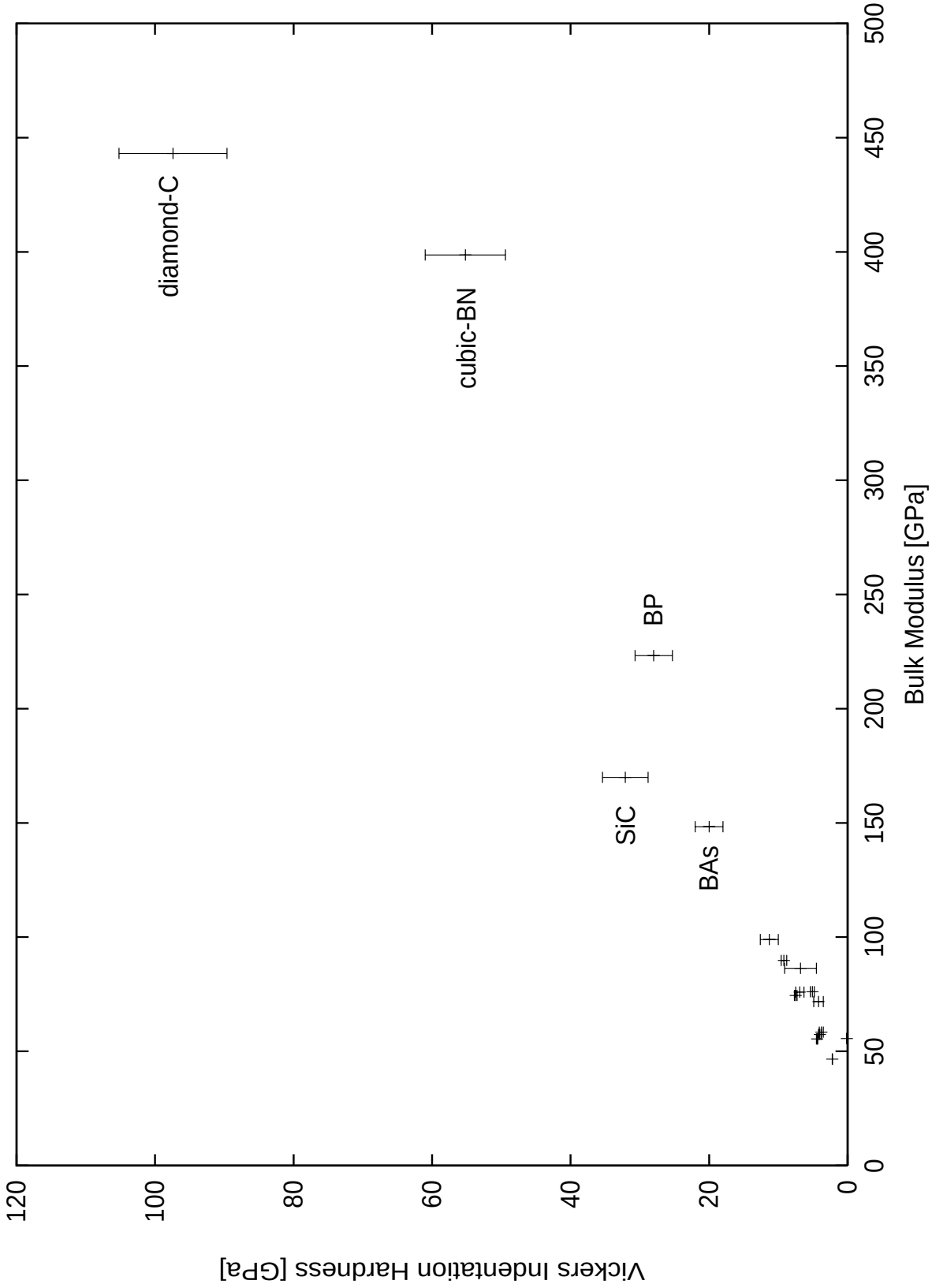

Figure 1.2: Hardness vs. bulk modulus for Group IV and Group III-V tetrahedral semiconductors.

Table 1.1: Bond lengths and bond stretching force constants for some chemical bonds between first and second row atoms.

Chemical Bond	Bond Length (Å)	Force Constant (N/m)	Origin
^{IV}N-O	1.26	839	H_3NO_4
^{IV}C-O	1.37	717	H_4CO_4
^{IV}C-N	1.44	610	H_8CN_4
^{IV}B-O	1.46	638	H_5BO_4
^{IV}C-C	1.54	502	diamond–C
^{IV}B-N	1.57	432	cubic–BN
^{IV}Si-O	1.63	600	H_4SiO_4
^{IV}Si-N	1.72	492	H_8SiN_4
^{IV}Si-C	1.87	297	3C–SiC

$$K_0 = \frac{\sqrt{2} f_c(MX)}{R(MX)}. \tag{1.1}$$

The bond lengths and quadratic–bond–streching force constants for a selected number of chemical bonds consisting of first– and second– row atoms of the perodic table are given in Table 1.1. According to Eq. 1.1, the bulk modulus of a material with a structure like diamond should increase with increasing force–constant and decreasing bond length. Hence, it would seems reasonable that materials in the B–C–N–O chemical system with diamond like structures might serve as promising candidates as superhard materials.

Additional constraints that must be considered in our search for superhard materials is the number of valence electrons of the atoms in the material and its stoichiometry. Superhard materials with the diamond structure tend to obey electron counting rules in which the average number of valence electrons per lattice site is four.[66, 67, 156, 233] A number of "symmetrical" isoelectronic compounds such as cubic–BN (a III-V analog of diamond and the second hardest known material[37]) and SiC have been synthesized and are important

hard materials. An interesting class known as "unsymmetrical periodic compounds" has been described by Hall[66, 67], following the synthesis of a graphite modification of B_2O at high-pressure.[67] B_2O is isoelectronic with diamond with each formula unit containing two boron atoms with 3 valence electrons each and one oxygen atom with 6 valence electrons. This leads to an average number of 4 valence electrons per atom, therefore, B_2O is isoelectronic with diamond and may display similar properties. Hall describes an entire class of binary and ternary "unsymmetrical" compounds that are isoelectronic with diamond.[66, 67])

In a subsequent study, Zhogolev *et al.* extended Hall's ideas in considering defect structures that are isoelectronic with that of diamond.[233] One material suggested as being potentially superhard is C_3N_4, a material that is isoelectronic with diamond. It consists of 3 carbons with 4 valence electrons per atom and 4 nitrogens with 5 valence electrons per atom. This leads to a total of 32 electrons distributed among 8 lattice sites. If we consider C_3N_4 to possess the defect-zincblende structure, then each carbon atom is bonded to 4 nitrogen atoms, while each nitrogen atom is bonded to 3 carbon atoms and also possesses a non-bonding orbital (lone pair) oriented towards the defect site. Some of the more interesting compounds suggested by Zhogolev *et al.*[233] are given in Table 1.2.

1.2.2 Generating a Set of Reasonable Crystal Structures

A wide variety of methods are available for generating promising model crystal structures for superhard materials. Comparative crystallography is the process of considering known structures from chemically analogous systems to use as model structures.[73, 80, 115, 224] For example, the prediction of high pressure phases of SiO_2 have drawn on known dense stoichmetrically similar phases as potential structures for silica. This technique has been used quite successfully for predicting possible post–stishovite phases in SiO_2 by considering

Table 1.2: Two– and three–component systems isoelectronic with diamond recommended by Zhogolev *et al.* for the synthesis of new superhard materials.

System	Lattice sites/cell	Vacancies/cell
C_3N_4	8	$-\frac{1}{8}$
$C_{11}N_4$	16	$-\frac{1}{16}$
BC_2N	4	0
BC_6N	8	0
$B_3C_2N_3$	8	0
B_2CO	4	0
B_2C_5O	8	0
B_5NO_2	8	0

the crystal structures found in analogous metal dioxide, dichloride and difluoride systems as candidate structures. While, this technique can be quite valuable, it is limited by the availability of known structures; the structures must also be viable for the system of interest.

Global minimization techniques such as simulated annealing strategies that search for interesting local and global minima using a potential energy function are very robust methods for the generation novel structures.[12, 35] However, they can be quite computationally expensive and are not currently efficient strategies for generating candidate structures using energies derived from first–principles calculations. These methods can also be severely limited by the ability to develop a interatomic potential that accurately describes the bonding in the chemical system of interest.

Several methods exist that reduce the complexity of the structure generation problem by taking advantage of the underlying topology of the cation network of crystal structure. An example of this process is the use of algorithms based on the concept of crystalline nets to generate new structures.[224] For example, we can derive new tetrahedrally–coordinated structures for silica by only considering possible tetrahedral nets dictated by known geomet-

rical constraints .[35] New forms of silica are derived in this process by placing oxide anions half way betwen each Si atom of the net and optimizing the resulting tetrahedral framework with distance leasts squares startegies. The inverse of this process can also be used to generate new crystal structures for Si metal by removing the oxide anions from known framework structures such as the silica polymorphs, feldspars, the zeolites and the clathrates. As shown in Figure 1.3, the underlying tetrahedral silicon–net in the high–cristobalite structure of SiO_2 is isostructural with diamond while the tetrahedral net of high–tridymite is isostructural with that of lonsdaleite (hexagonal–diamond). Other topological relationships also exist between the keatite–SiO_2 and ST12–silicon structures as well as the melanophlogite–SiO_2 and the SC46–silicon clathrate. We can use this reverse relationship to generate new structures for carbon or silicon from the underlying silicon nets found in the silica structures. This process has also been used to derive a possible high pressure phase of carbon (H3) from the silicon net found in quartz.[200]

The tendency of many materials to possess structures that are based in part or entirely on a close packing of its atoms can also be used as an algorithm in the generation of new crystal structures.[80, 115, 224, 201] A large number of crystal structures can be visualized either in terms of close–packed arrays (either *hcp* or *ccp*, or mixtures of the two stacking sequences) of anions or cations. For each ion in the array, there are two available tetrahedral interstices and one available octahedral interstice. If these interstices are occupied by cations, the close–packed arrays of anions are usually distorted from ideal packing by bonded interactions between adjacent cations and anions, and by cation–cation and anion–anion antibonding and nonbonding interactions. This follows from the concept of eutaxy, which states that structures adopt these packings because they tend to maximize the anion–anion and cation–cation separations while maintaining a near ideal cation–anion bond lengths [151]. For example, the close packed $CaCl_2$ modification of SiO_2 (Fig. 1.4) can be described as a

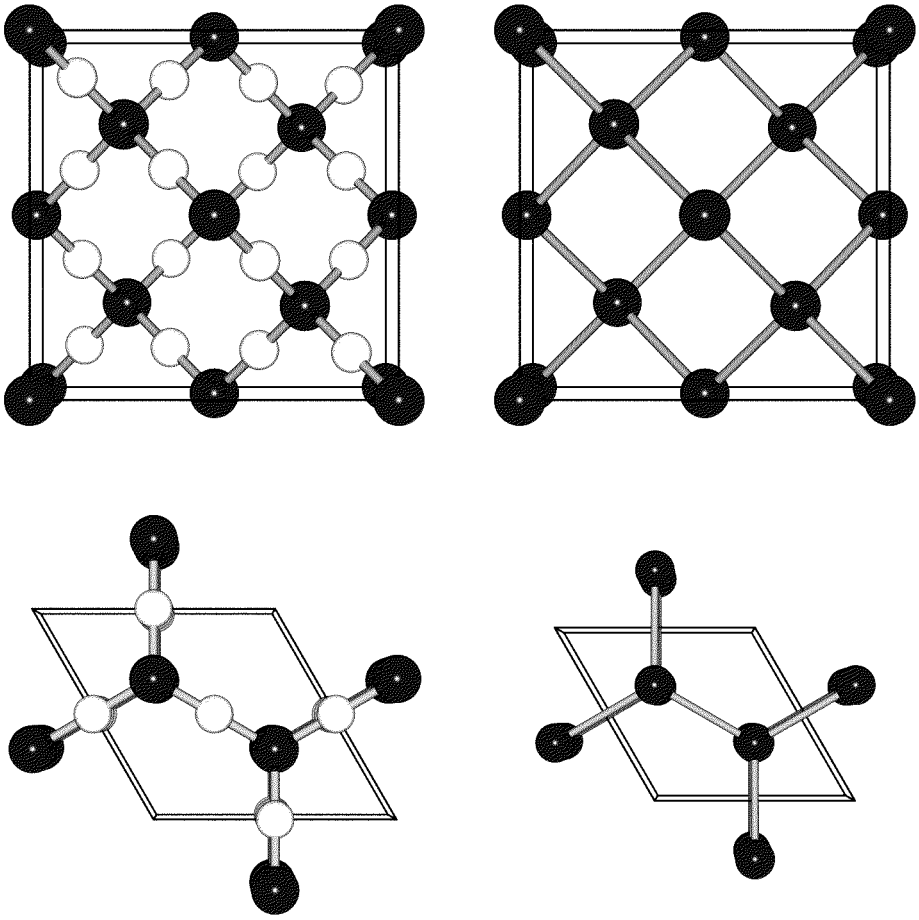

Figure 1.3: Representations of the (a) high–cristobalite, (b) diamond, (c) high–tridymite and (d) lonsdaleite crystal structures.

hcp array of oxygen ions with one-half of the available octahedral interstices occupied by silicon. This gives rise to straight chains of edge–sharing SiO_6 octahedra that are corner linked between ($\cdots$ABAB$\cdots$) layers to form a three dimensional network. The α–PbO_2 structure–type of SiO_2, which is observed as a post–rutile phase in a number of analog systems, can also be described in terms of a *hcp* packing of oxygen. However, in this case the silicon cations are arranged in such a way as to generate 2x2 zigzag chains of edge–sharing octahedra. The MX superstructures for hexagonal and cubic close-packing are the NiAs and NaCl structure types. In both structures, cations occupy all of the octahedral sites

between the close–packed anion layers. The removal of one-half of the M ions from the NiAs structure can lead to the generation of the rutile and α–PbO_2 structures, while the anatase structure can be derived by removing one-half of the M atoms from the NaCl structure. Novel framework structures of MX_6 octahedra can be generated by constructing NiAs or NaCl–type supercells, or combinations of their stacking variants, and removing one-half of the metal ions according to simple rules [224, 201].

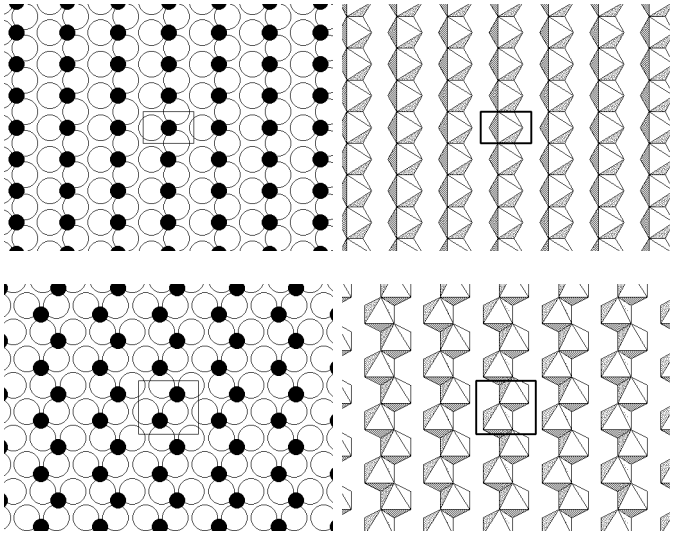

Figure 1.4: Representations of the (a) $CaCl_2$ and (b) α–PbO_2 structure types of SiO_2. The left–hand figures show one layer of the $ABAB...$ stacking of *hcp* oxygen anions (white) with one–half of the octahedral interstices filled with silicon ions (black). The right–hand figures show how these patterns form edge–sharing octahedral chains with various degrees of kinking.

1.2.3 Selecting a Method for Calculating Energies

In the determination of the properties of new materials, we use first–principles total–energy electronic structure computational methods. The prediction of the physical properties of a solid requires minimizing the quantum–mechanical total–energy of the solid with repect to the electronic and nuclear coordinates of its atoms. Because the mass of the electrons is significantly less the mass of the nuclei, we can assume that the the electrons respond instantaneously to changes in nuclear motion. This assumption, known as the Born–Oppenheimer approximation, allows the nuclei to be treated adiabatically and allows a separation of the electronic and nuclear coordinates in the many–body wavefunction. This reduces the many–body problem to the solution of the electronic coordinates in some "frozen" configuration of nuclei. We use a series of approximations to reduce the many–problem to one that is tractable, yet still accurate. The density–functional theory is uded to model the electron–electron interactions and the pseudopotential theory is used to model electron–ion interactions.

The density functional theory of Hohenberg and Kohn[77] states that for a given external potential, such as the Coulomb potential, the total energy of an electronic system is a functional of the electronic density. This energy is variational as small deviations of the electronic density from the ground state increase the total energy. Therefore, the ground–state energy of a system can be determined by searching though the possible electronic densities until the total energy is minimized. Kohn and Sham showed that the electronic density could be constructed from single–electron orbitals.[97] This reduces the problem of describing a strongly interacting electron gas in the precence of nuclei to that of a single particle moving in an effective local potential. While the exact functional form of this potential is unknown, local approximations to it such as the local density approximation works rather well and reproduces the physical properties of a large class of materials to

within a few percent of their experimental values.

Pseudopotential theory allows the strong electron–ionic potential to be replaced by a much weaker potential that describes the potential seen by a valence electron moving through the solid. The original solid is now constructed of pseudo–ion cores and pseudoelectrons. However, while these pseudoelectrons experience the same potenitial outside the core region, they have a much weaker potential inside the core. This allows the wavefunctions to be expanded into a relatively small set of plane waves and greatly simplifies the solution to Schrödinger's equation. The use of plane waves as basis functions also greatly simplifies the calculation of the ionic forces and stresses on the unit cell.

1.2.4 A Calculation of the Bulk Modulus

In this section, the strategy used to calculate the zero pressure bulk modulus of a material is discussed. In the calculation, the total energy and unit cell volume of a material are fit to the Birch equation of state [11].

$$E_{total} = \sum_{n=1}^{N} a_n V^{-2n/3} \tag{1.2}$$

where E_{total} is the total energy and V is the unit cell volume. Truncating the series after the n=3 term, we have the expression

$$E = a_1 + \frac{a_2}{V^{2/3}} + \frac{a_3}{V^{4/3}} + \frac{a_4}{V^{6/3}} \tag{1.3}$$

The pressure, P, can then be obtained from this relationship by evaluating the derivative of the energy with respect to the volume.

Table 1.3: Comparison of theoretical and experimental cubic–BN bulk moduli

	a [$\mathring{A}$]	K_0 [GPa]	K'
Calc.	3.574	394.7	3.62
Expt.	3.615	400.0	4.00

$$P = -\frac{\partial E}{\partial V} = \frac{2}{3}\frac{a_2}{V^{5/3}} + \frac{4}{3}\frac{a_3}{V^{7/3}} + 2\frac{a_4}{V^3} \tag{1.4}$$

and the bulk modulus (K) given by

$$K = -V\frac{\partial P}{\partial V} = -V\left(-\frac{10}{9}\frac{a_2}{V^{8/3}} - \frac{28}{9}\frac{a_3}{V^{10/3}} - 6\frac{a_4}{V^4}\right) \tag{1.5}$$

Finally, the pressure derivative of the bulk modulus (K') is given by the expression

$$K' = \frac{\partial K}{\partial P} = \frac{\frac{10}{9}\frac{a_2}{V^{8/3}} + \frac{28}{9}\frac{a_3}{V^{10/3}} + 6\frac{a_4}{V^4} - V\left(\frac{80}{27}\frac{a_2}{V^{11/3}} + \frac{280}{27}\frac{a_3}{V^{13/3}} + 24\frac{a_4}{V^5}\right)}{-\frac{10}{9}\frac{a_2}{V^{8/3}} - \frac{28}{9}\frac{a_3}{V^{10/3}} - 6\frac{a_4}{V^4}} \tag{1.6}$$

To illustrate such calculations, we have calculated the energies over a wide range of unit cell volumes for cubic–BN. If we take the calculated energies and the respective volumes from Table **??** and fit them to Equation 1.3, we obtain the following fitting parameters: a= 18.0903, b= -411.069, c= 1271.15, and d= -775.174. The calculated zero–pressure a–cell edge, bulk modulus (K_0), and bulk modulus pressure derivative (K_0'), evaluated for the zero pressure unit cell volume (Table 1.3) are in excellent agreement with the experimental values.

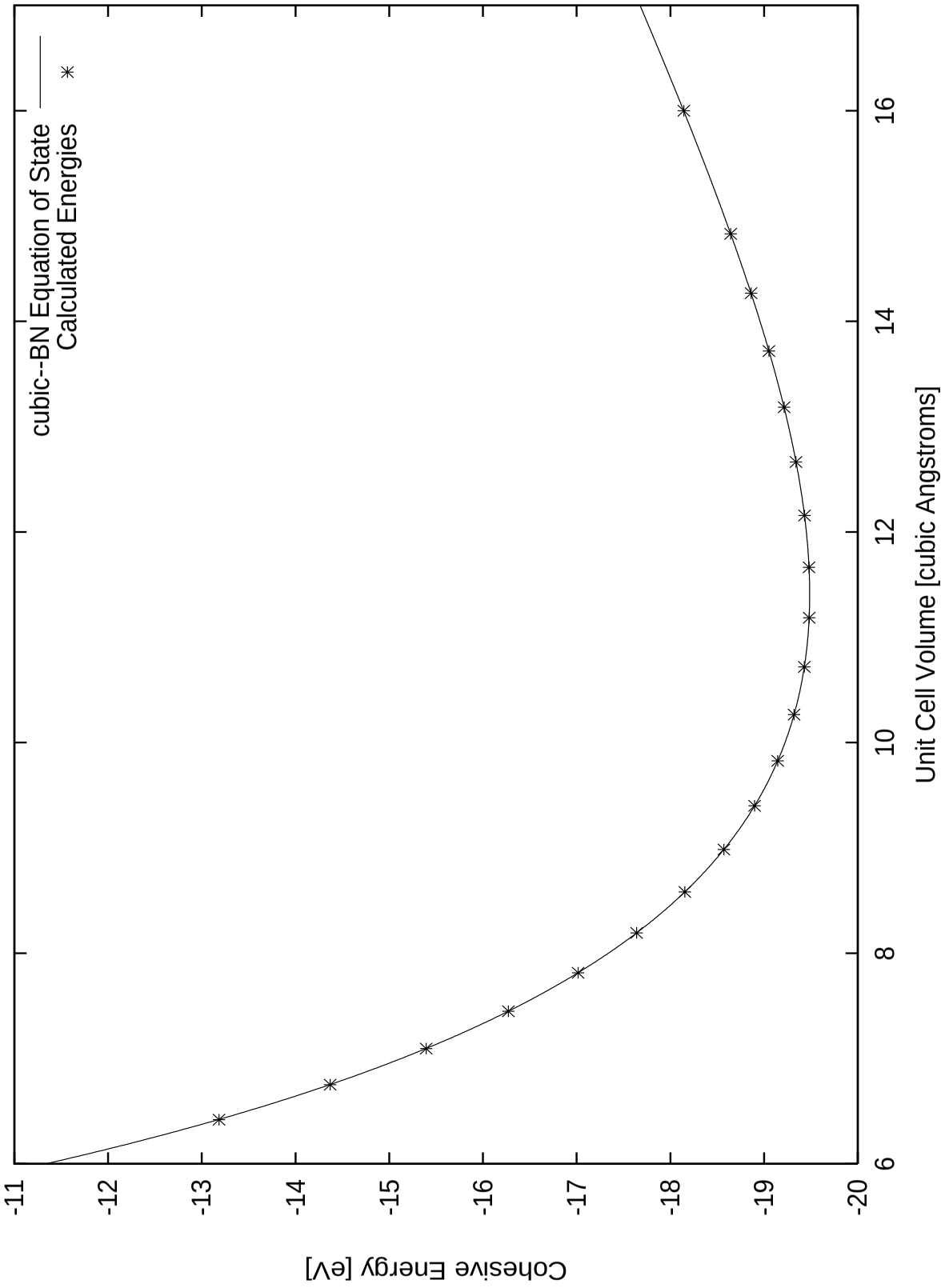

Figure 1.5: Energy-volume curve for cubic–BN.

Chapter 2

Determining a Better Figure of Merit for Predicting Hardness

"Hardness, like the storminess of the seas, is easily appreciated but not readily measured."

-H. O'Neill[153]

2.1 Introduction

Hardness is not only difficult to measure, it is difficult to define. It is a quality that is defined in terms of how it is measured; hence, there are as many kinds of hardness as there are ways of measuring it.[81, 132, 153, 179, 191, 192, 193, 194, 195] However, in a general sense, hardness can be thought of as "the resistance offered by a given material to external mechanical action looking to scratch, abrade, indent or in any other way permanently affect its surface."[191]

The hardness of a material is ultimately defined at the atomic level. A rigid crystal should be more resistant to deformation than a compliant one. To relate the crystal structure of a material to its hardness, both the strength of the chemical bonds and the rigidity of the bonding network need be considered as it is possible to have a compressible crystals with very strong bonds (for example, consider the α–cristobalite polymorph of SiO_2 which contains rigid, strongly bonded SiO_4 silicate tetrahedra linked together into a 3D framework by compliant SiOSi angles). In such a case, high compressibility of cristobalite can be related to the compliant nature of the SiOSi angle. Early attempts at an atomic definition of hardness were worked out by Goldschmidt in which the atomic valences and bond distances were considered. Since then, such physical properties as the "volumetric lattice energy"[57, 162], bond–ionicity, melting point[96], and band gap[49, 51] have also been used to predict hardness with varying degrees of success. An alternative approach is to consider the elastic properties of a material. These properties, such as the bulk, shear, and elastic modulus are defined by the elastic constants of a crystal. The elastic constants of a crystal can not only be measured in a variety of ways, but they can also be calculated accurately using first–principles methods.[136] The elastic properties of a material are influenced by both the strength of the bonds and the topology of the crystal structure. In effect, they are governed by a crystal's ability to resist hydrostatic compression, tensile load, and shear, and relate to its resistence to plastic flow. As mentioned previously, several hundred recent experimental efforts to synthesize and study new superhard materials have been initiated based upon theoretical predictions that certain carbon nitrides have zero pressure bulk moduli that approach[23, 116, 118, 119, 154, 166, 197, 230] and even exceed[197] that of diamond. If the K_0 is universal measure of hardness, then the carbon nitrides should qualify as superhard materials. [26, 53, 110, 116, 163, 189, 229] But, as will be demonstrated below, there are materials like HfN, for example, that has a large bulk modulus of 422 GPa yet its Vicker hardness (17 GPa) is a less than one–fifth that of diamond (97 GPa). Given these results,

clearly a new figure of merit that is more universal than the bulk modulus is required for identifying superhard materials.

2.2 Determining a Better Predictor of Hardness

Given the large bulk modulus of materials like HfN and its relatively low hardness, it is clear that hardness of materials is not universally governed by their bulk moduli. In effect, the bulk modulus is not a good figure of merit for predicting hardness. In many hardness tests, plastic deformation of the material is measured that appears to be closely linked to deformation of a shear character, one which is initially elastic but in later stages displays yield. This cannot simply be related to a reversible and purely volume dependent deformation. It has therefore been suggested that the shear modulus (the resistance to reversible deformation upon shear), might well be a better predictor of hardness, more securely rooted in the nature of the actual deformation processes.[43, 47, 198] Because these deformations are not reversible, it cannot be expected that this relationship is direct, but more likely it is related to the activation and mobility of an associated dislocation network. It is the resolved shear stress that governs the activation of dislocations, and their mutual interactions that are then involved in their subsequent mobility. To test this proposition, a large data set of hardness values and elastic properties has been assembled from several thousand measurements (Table 2.1 summarizes the averaged data, while the raw data is presented in Appendix 2).[198]

We compare the hardness values for all with the zero pressure bulk moduli (Fig. 2.1), shear moduli (Fig. 2.2), elastic moduli (Fig. 2.3), atomic density (Fig. 2.5), volumetric cohesive energy (Fig. 2.6, and band gap (Fig. 2.7. It can be readily seen that the shear modulus is a significantly better qualitative predictor of hardness than the bulk modulus. The elastic modulus is also a better predictor of hardness than the bulk modulus, but this

is not surprising, as the elastic modulus is highly correlated with the shear modulus. This relationship can be understood from Equation 2.1 and observed in Figure 2.4.

$$\frac{1}{E} = \frac{1}{9K} + \frac{1}{3G} \tag{2.1}$$

In the search for new superhard materials, it would therefore seem worthwhile to concentrate attention on materials with high shear moduli rather than those with large bulk moduli.

Physical Properties database

Material	VHN (GPa)	K_0 (GPa)	G_0 (GPa)	E_0 (GPa)	ρ_{atomic} (atoms/Å^3)	$\frac{H}{\nu}$ (GPa)	E_{gap} (eV)
C	97.1 ±7.0	443.3 ±1.3	534.7 ±0.7	1144	0.1761	209.2	5.4
SiC	28.1 ±2.8	220.3 ±7.7	191.1 ±5.0	445.7	0.0966	99.4	3.1
Si	11.3 ±1.2	98.9 ±1.0	65.3 ±2.7	160.6	0.0499	37.6	1.1
Ge	7.7 ±0.4	74.4 ±3.2	54.9 ±0.7	132.2	0.0442	27.5	0.7
Sn	0.1 ±0.0	55.6 ±1.7	18.0 ±0.0	48.7	0.0293	14.6	0.1
BN	47.8 ±8.7	399.0 ±8.6	408.5 ±7.9	913.7	0.1692	180.6	5.7
BP	32.1 ±3.3	166.4 ±7.3	155.2 ±26.5	355.2	0.0856	71.7	2.0
BAs	20.0 ±2.0	148.3 ±2.5	-	-	0.0734	-	1.5
AlN	12.8 ±0.8	203.1 ±7.4	128.6 ±7.3	318.6	0.0959	89.2	6.2
AlP	6.8 ±2.3	86.3 ±0.6	52.0 ±0.0	129.9	0.0491	34.0	2.4
AlAs	5.1 ±0.3	76.1 ±1.6	45.3 ±0.8	113.4	0.0441	27.4	2.2
AlSb	4.0 ±0.2	57.4 ±1.8	32.2 ±0.4	81.4	0.0346	18.5	1.6
GaN	12.3 ±2.6	199.6 ±10.2	120.1 ±3.9	300.1	0.0876	62.0	3.5
GaP	9.2 ±0.4	89.8 ±3.0	55.6 ±0.2	138.3	0.0494	29.0	2.3
GaAs	6.9 ±0.6	75.9 ±1.0	46.6 ±0.2	116.0	0.0443	20.8	1.4
GaSb	4.4 ±0.1	55.4 ±1.6	34.2 ±0.0	85.1	0.0353	17.0	0.7
InN	10.0 ±0.0	143.2 ±3.2	55.7 ±2.1	147.9	0.0645	46.3	2.0
InP	4.2 ±0.7	71.8 ±1.0	35.4 ±1.4	91.2	0.0396	22.0	1.3
InAs	3.8 ±0.3	58.4 ±0.7	29.5 ±0.0	75.7	0.0360	18.1	0.4
InSb	2.2 ±0.0	46.6 ±0.8	22.9 ±0.0	59.0	0.0294	13.2	0.2
BeO	11.8 ±1.0	250.0 ±1.0	160.9 ±1.3	397.4	0.1449	142.1	10.7
ZnO	4.4 ±0.4	144.0 ±3.9	45.7 ±1.4	124.0	0.0840	48.9	3.3
ZnS	1.8 ±0.1	75.9 ±1.5	32.9 ±1.2	86.2	0.0505	25.7	3.6
ZnSe	1.4 ±0.3	62.5 ±3.0	29.4 ±0.4	76.2	0.0439	19.5	2.7
ZnTe	1.0 ±0.1	51.2 ±0.4	23.5 ±0.1	61.2	0.0352	13.5	1.9
CdS	0.7 ±0.1	62.6 ±1.5	16.9 ±0.3	46.4	0.0402	18.2	2.6
CdSe	0.8 ±0.1	53.4 ±0.5	15.5 ±0.5	42.5	0.0356	15.1	1.8
CdTe	0.5 ±0.1	42.5 ±0.5	14.1 ±0.1	38.2	0.0293	10.3	1.5
CrB	21.6 ±2.6	-	-	-	0.1176	101.3	0.0
CrB_2	20.6 ±2.6	-	-	-	0.1276	116.1	0.0
HfB_2	27.6 ±4.1	223.0±0.0	-225.0±0.0	-	0.1014	116.1	0.0
MoB	24.3 ±0.8	-	-	-	0.0978	109.0	0.0
MoB_2	18.3 ±5.3	-	-	-	0.1221	123.4	0.0
NbB_2	24.5 ±3.0	-	-	-	0.1099	-	0.0
TaB_2	24.5 ±2.3	-	-	-	0.1126	-	0.0
TiB_2	32.9 ±2.7	240.7 ±7.7	247.1 ±7.8	552.3	0.1167	123.3	0.0
VB_2	23.4 ±3.1	-	-	-	0.1276	127.8	0.0
WB	26.1 ±0.7	-	-	-	0.0974	117.7	0.0
ZrB_2	23.5 ±3.2	207.7 ±0.0	205.7 ±13.9	463.9	0.0977	110.6	0.0
Cr_3C_2	13.9 ±2.2	-	-	-	0.1114	104.9	0.0
Fe_3C	7.0 ±0.0	-	-	-	0.1030	82.6	0.0
HfC	24.5 ±3.5	271.5 ±0.0	217.0 ±53.7	514.0	0.0800	103.7	0.0
Mo_2C	17.5 ±1.7	-	-	-	0.0812	93.5	0.0
NbC	22.9 ±3.4	298.4 ±2.7	206.2 ±10.6	502.8	0.0939	123.8	0.0
TaC	18.0 ±2.1	217.0 ±0.0	118.0 ±0.0	299.7	0.0910	124.1	0.0
TiC	28.9 ±2.8	241.0 ±1.4	185.9 ±10.7	443.6	0.0986	112.6	0.0
UC	7.2 ±1.9	163.0 ±0.0	83.0 ±0.0	212.9	0.0659	73.1	0.0
VC	24.2 ±3.9	343.0 ±5.4	232.6 ±0.0	569.1	0.1107	-	0.0
WC	24.0 ±3.0	427.5 ±9.2	276.0 ±8.5	681.4	0.0962	126.7	0.0
ZrC	25.6 ±5.4	202.4 ±28.5	165.2 ±1.7	389.6	0.0786	99.5	0.0
CrN	15.5 ±6.6	-	-	-	0.1127	92.4	0.0
HfN	19.0 ±3.1	422.0 ±0.0	141.0 ±0.0	380.6	0.0867	97.5	0.0
NbN	16.2 ±3.9	286.7 ±0.0	153.8 ±3.1	391.4	0.0943	112.8	0.0
TaN	27.6 ±0.5	383.0 ±0.0	-	-	0.0984	110.2	0.0
TiN	20.3 ±1.1	295.1 ±16.5	201.1 ±19.7	491.6	0.0939	100.1	0.0
VN	14.7 ±1.1	267.7 ±0.0	147.7 ±8.0	374.3	0.1136	-	0.0
UN	6.5 ±0.0	206.7 ±0.0	103.5 ±0.0	266.1	-	-	0.0
ZrN	17.6 ±2.1	276.7 ±0.0	159.0 ±0.0	400.3	0.0806	96.5	0.0
Al_2O_3	22.7 ±2.5	250.9 ±6.4	161.6 ±2.8	399.1	0.1181	120.4	4.1
$Al_2SiO_4(F,OH)_2$	3.9 ±0.5	167.0 ±0.0	115.0 ±0.0	280.6	-	-	-
B	31.3 ±4.0	235.0 ±0.0	208.0 ±0.0	472.8	0.1278	118.9	1.7
B_4C	32.9 ±5.7	250.4 ±4.3	186.5 ±1.6	448.2	0.1367	137.0	-
B_60	35.1 ±4.6	228.0 ±0.0	204.0 ±0.0	471.4	0.1366	-	2.4
Be_2SiO_4	14.6 ±0.0	212.8 ±2.5	99.0 ±0.0	256.2	-	116.7	-
$Ca_3Al_2Si_3O_{12}$	13.3 ±0.4	170.0 ±0.0	100.0 ±0.0	250.8	-	-	-
$CaCO_3$	1.5 ±0.4	72.0 ±1.0	32.0 ±0.0	83.6	-	-	-
CaO	6.5 ±0.5	112.4 ±1.6	80.9 ±0.4	196.1	-	63.6	-
$Ca_{10}PO_4F_2$	5.3 ±0.0	212.0 ±0.0	102.0 ±0.0	263.7	-	-	-
$CaWO_4$	3.8 ±0.4	76.5 ±0.0	37.4 ±0.0	6.5	-	-	-
CoO	3.6 ±0.4	183.3 ±0.0	71.3 ±0.0	89.3	-	-	-
Fe_2O_3	9.3 ±1.2	213.0 ±13.5	91.0 ±0.0	239.0	0.0997	78.9	-
Fe_3O_4	5.7 ±0.3	177.5 ±11.2	91.2 ±0.2	233.6	-	75.2	-
$FeCr_2O_4$	12.2 ±0.3	203.3 ±0.0	104.9 ±0.0	270.1	-	-	-
FeS_2	11.0 ±2.5	149.3 ±7.1	126.0 ±0.0	295.0	0.0755	47.6	1.3
a–GeO2	2.4 ±0.0	24.7 ±0.0	17.8 ±0.0	43.1	-	-	-
$MgAl_2O_4$	14.3 ±2.3	197.3 ±0.8	108.4 ±0.1	272.8	-	103.5	-
MgO	9.4 ±1.3	160.9 ±3.9	130.0 ±0.8	307.2	0.1087	88.6	-
$MgSiO_3$	18.0 ±2.0	255.8 ±7.1	177.0 ±0.0	431.5	-	92.4	-
Si_3N_4	23.6 ±5.1	254.9 ±17.9	116.3 ±5.6	316.8	0.0960	90.8	-
a–SiO_2	6.2 ±0.0	36.9 ±0.0	31.0 ±0.0	2.7	-	-	10.0
SiO_2-q	11.5 ±0.7	37.3 ±0.7	44.3 ±0.4	5.1	0.0801	82.0	6.1
SiO_2-s	33.0 ±1.6	304.6 ±11.2	220.0 ±0.0	531.9	0.1290	132.8	6.0
SnO_2	10.6 ±0.3	214.1 ±7.5	102.0 ±0.0	264.1	0.0839	64.2	3.6
ThO_2	10.2 ±0.8	193.0 ±0.0	97.0 ±0.0	49.2	0.0669	87.5	-
TiO_2	10.8 ±0.9	208.0 ±11.7	112.0 ±0.0	284.9	0.0962	102.0	3.0
UO_2	7.1 ±1.1	211.0 ±2.8	86.3 ±3.1	227.8	-	57.0	-
ZrO_2	12.1 ±1.4	224.0 ±0.0	67.0 ±0.0	182.8	0.0860	109.2	-
$ZrSiO_4$	11.5 ±0.7	227.0 ±0.0	109.0 ±0.0	281.9	-	104.0	-
Tourlam	11.3 ±0.0	127.0 ±0.0	82.0 ±0.0	202.4	-	-	-

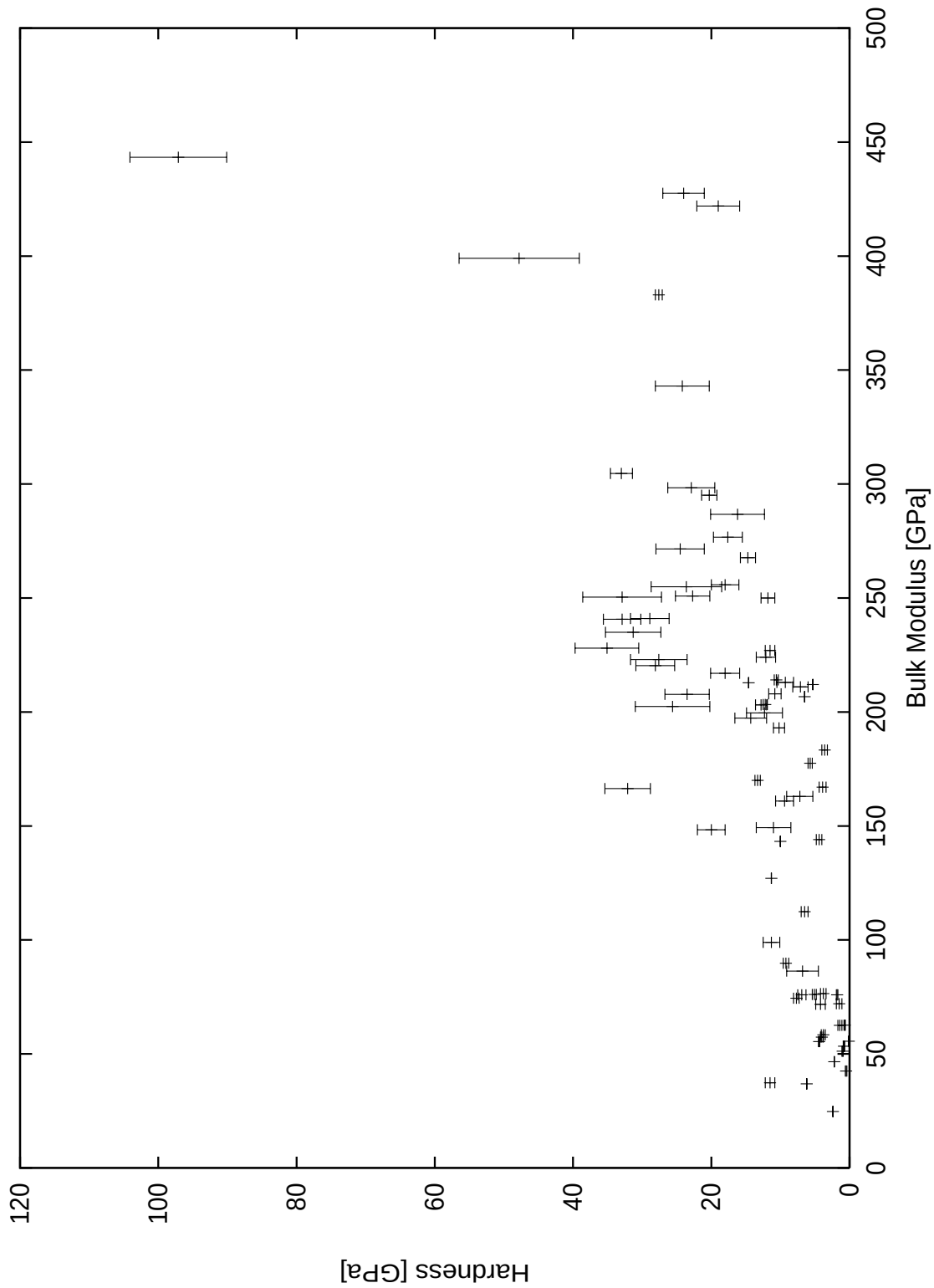

Figure 2.1: Comparison of hardness with the bulk moduli for a wide variety of hard oxides, nitrides, borides and carbides.

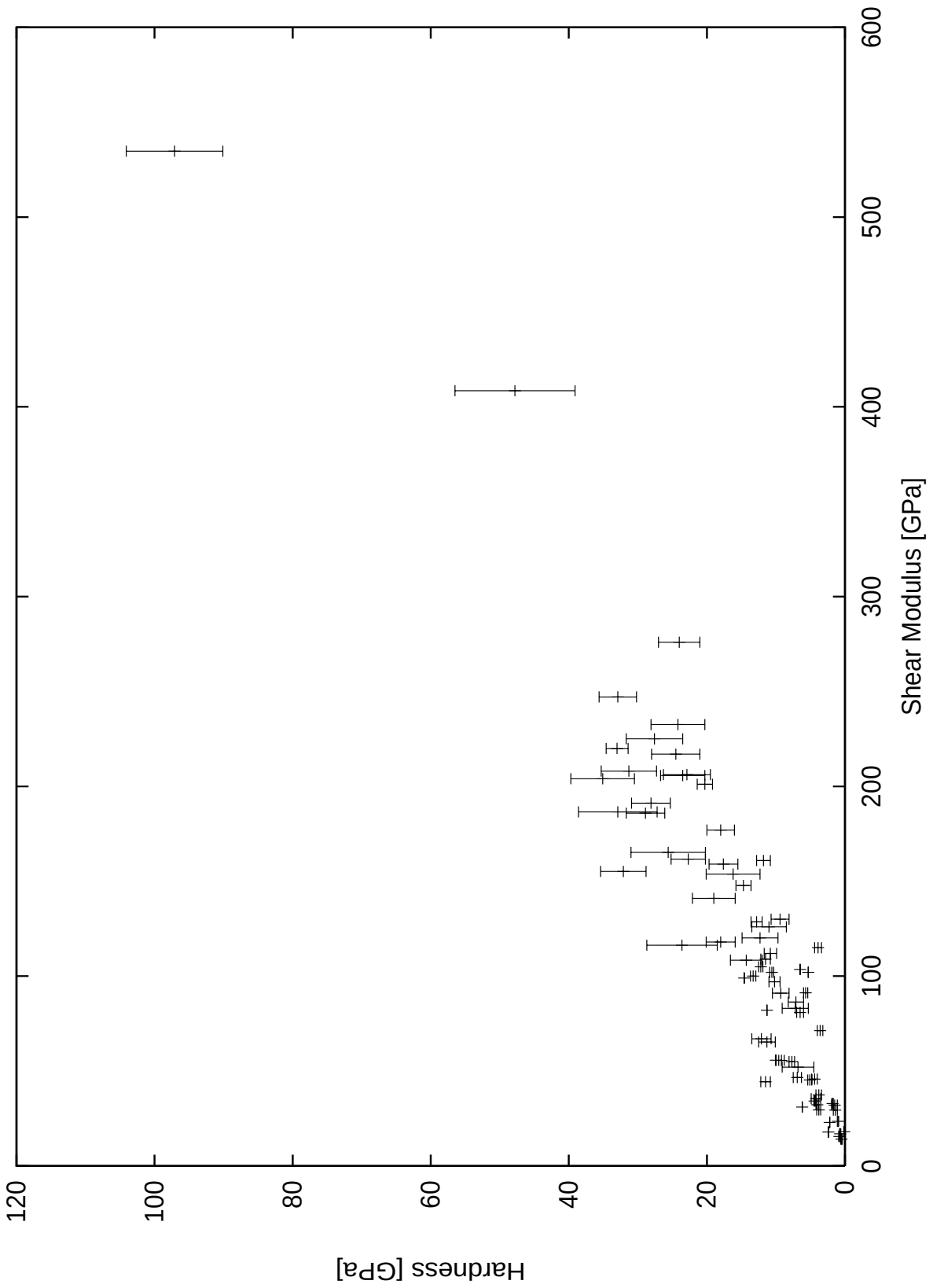

Figure 2.2: Comparison of the hardness with the shear moduli for a wide variety of hard oxides, nitrides, borides and carbides.

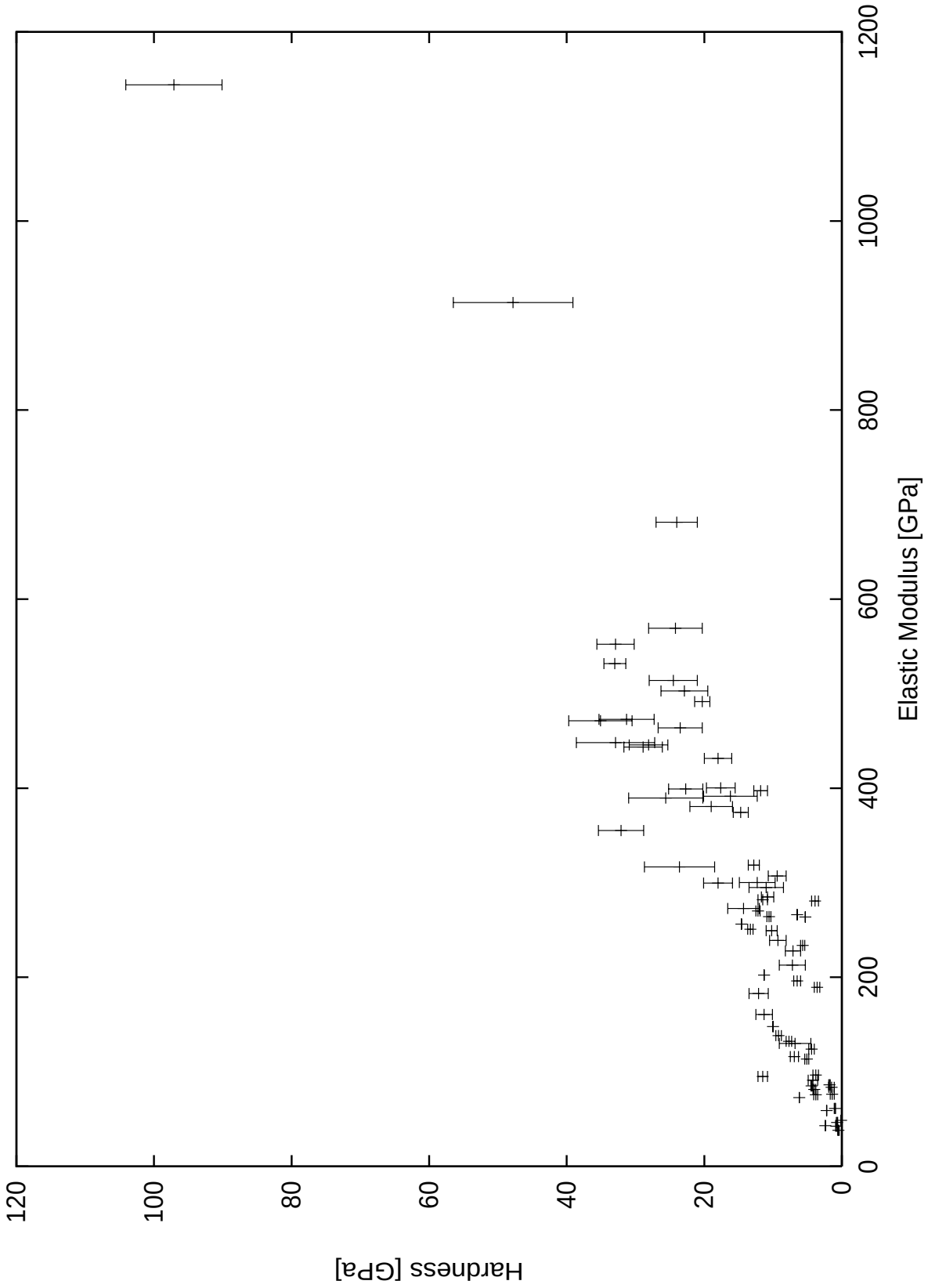

Figure 2.3: Comparison of the hardness with the Young's elastic moduli for a wide variety of hard oxides, nitrides, borides and carbides.

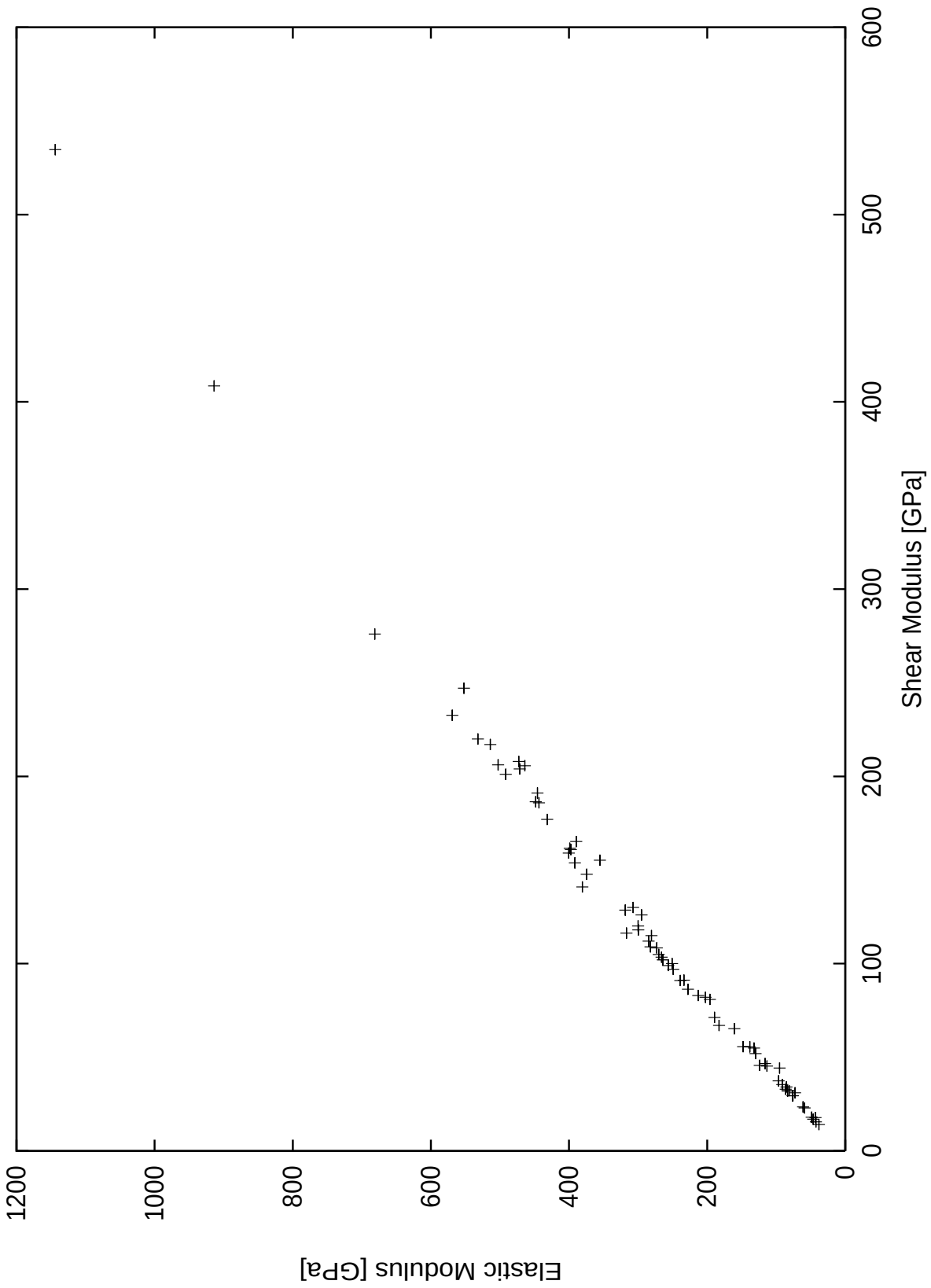

Figure 2.4: Comparison of the Young's elastic moduli with the shear moduli for a wide variety of hard oxides, nitrides, borides and carbides.

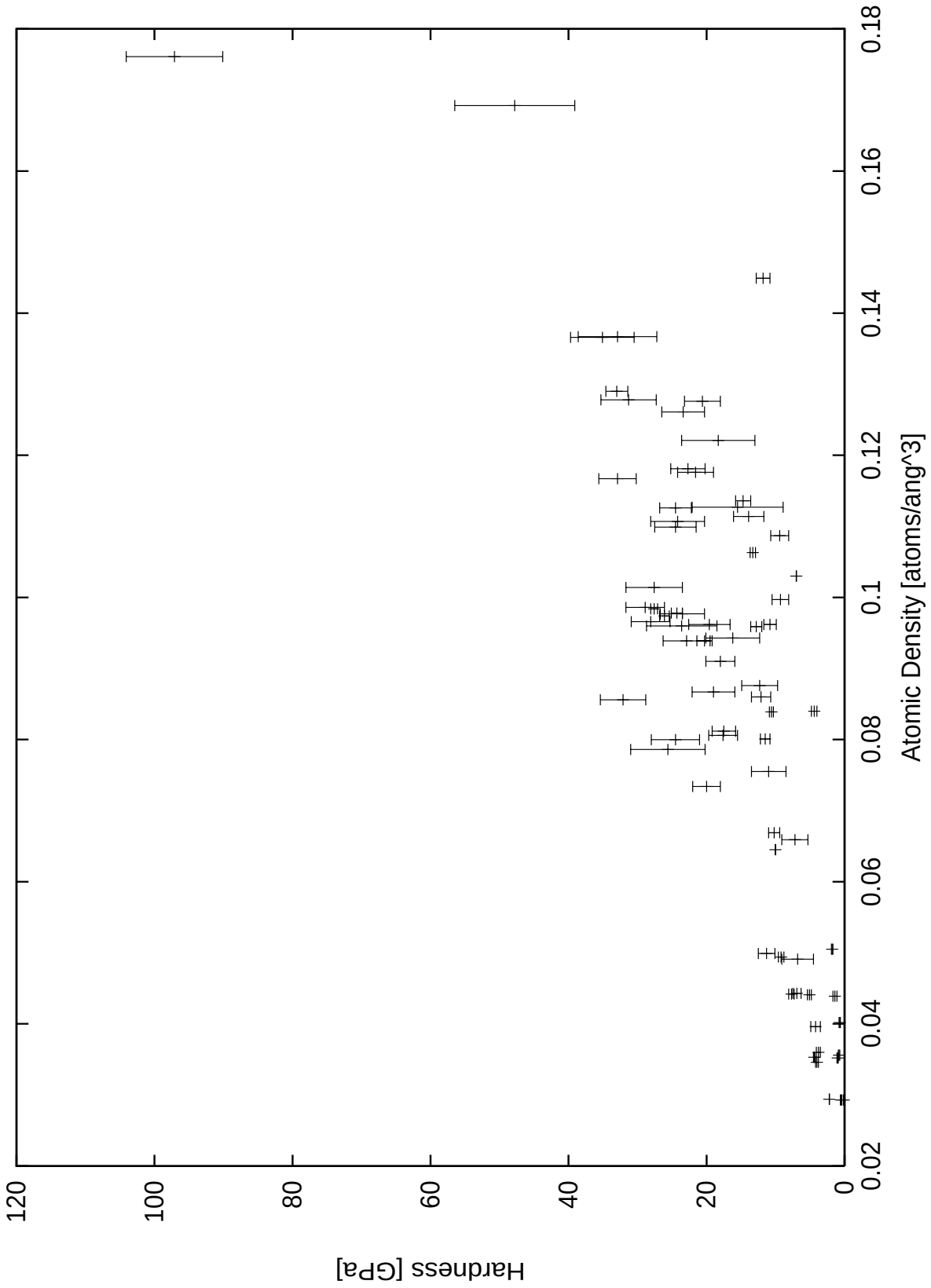

Figure 2.5: Comparison of the hardness with the atomic density for a wide variety of hard oxides, nitrides, borides and carbides.

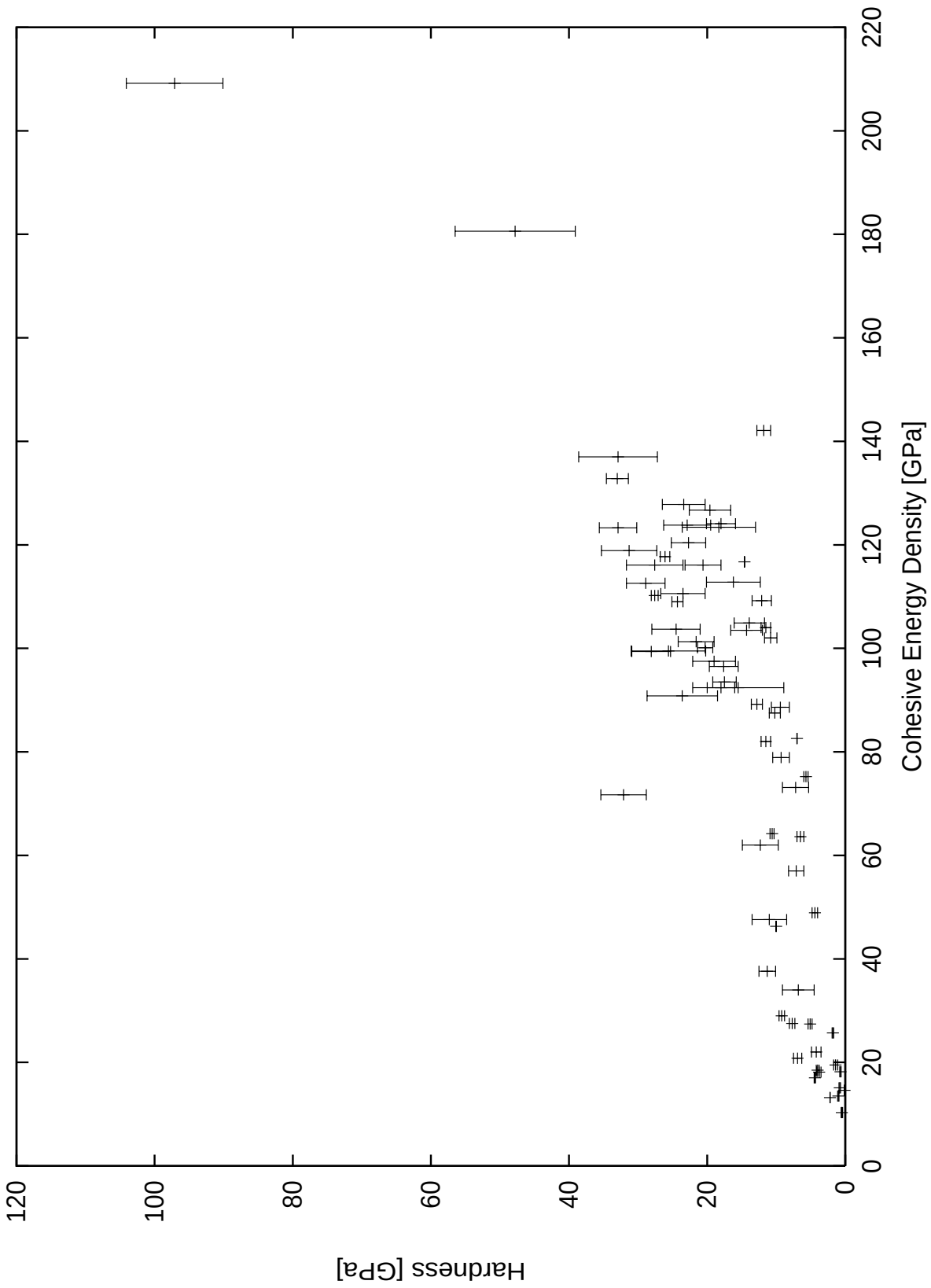

Figure 2.6: Comparison of the hardness with the cohesive energy density for a wide variety of hard oxides, nitrides, borides and carbides.

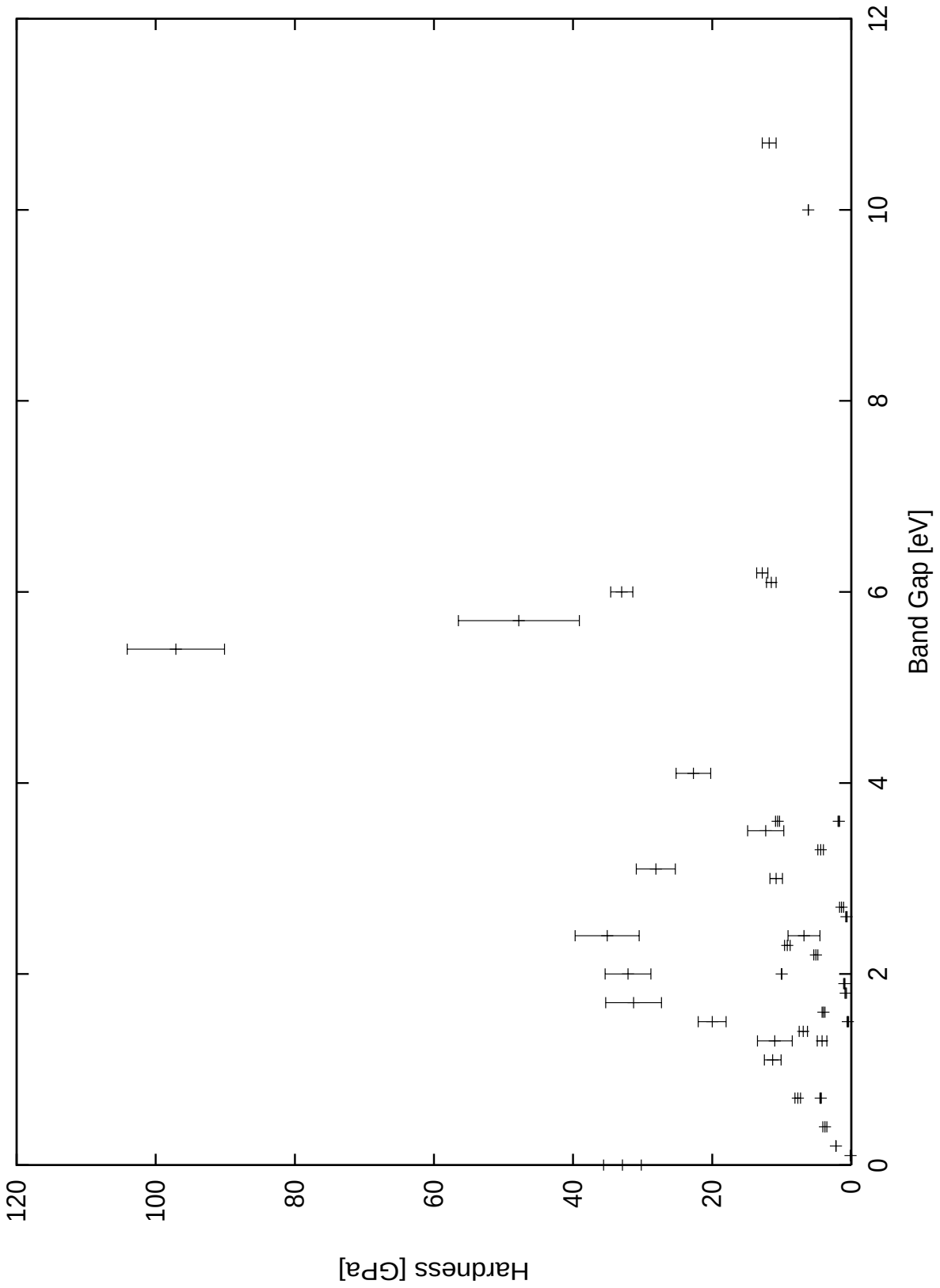

Figure 2.7: Comparison of the hardness with the band gap for a wide variety of hard oxides, nitrides, borides and carbides.

Chapter 3

Carbon Nitrides

3.1 Introduction

In 1985, Marvin Cohen developed an empirical expression that relates the bulk modulus of tetrahedrally coordinated materials to the length and ionicity of their chemical bonds. The resulting relationship is given by Equation 3.1 where d is the bond length and λ is a measure of the ionicity of the compound. For the Group IV semiconductors, λ=0, while for the Group III-V and II-VI zincblende structure, λ= 1 and 2, respectively. From this relationship, Cohen predicted that a tetrahedrally bonded material made from carbon and nitrogen should exhibit a bulk modulus higher than that of diamond due to the short length (d= 1.47 Å) and the high covalency (λ=$\frac{1}{2}$) of the C–N bond.[23]

$$B_0 = \frac{19.71 - 2.20\lambda}{d^{3.5}} \tag{3.1}$$

Subsequently, Liu and Cohen predicted that a modification of carbon nitride isostructural with β–Si_3N_4 possesses a bulk modulus approaching that of diamond.[116, 118] This result,

coupled with the statements that hardness is closely connected to the bulk modulus,[26, 53, 110, 116, 163, 189, 229] motivated numerous subsequent theoretical[3, 23, 32, 60, 69, 78, 116, 118, 119, 154, 166, 197, 230] and experimental efforts to study and synthesize the material. The interest in this work has been discussed in a series of reviews describing the search for superhard carbon nitrides.[4, 38, 42, 113, 112, 114, 128, 168, 173, 186, 189] While most of the initial work involved the search for β–C_3N_4, later theoretical studies demonstrated that a carbon nitride phase isostructural with α–Si_3N_4 is energetically preferable to β–C_3N_4 (albeit with very similar predicted properties).[60, 197] It has also been demonstrated that a defect–graphitic C_3N_4 compound appears to be the ground–state structure for this composition.[119, 154, 197] The α–, β–, and defect–zincblende–C_3N_4 structures all possess bulk moduli approaching that of diamond.

Table 3.1: Calculated structural zero–pressure structural parameters for the carbon nitride structures discussed in the text.

Structure	Atom	x	y	z
Rhom. graphitic–C_3N_4	C(1)	0.6843	0.8422	$\frac{1}{3}$
a=b=4.7310 Å, c=9.1660 Å	N(1)	0	0	0.6653
$R3m$ [160], Z=3	N(2)	0.32620	0.16310	$\frac{1}{3}$
E_{coh}= -65.334 eV/C_3N_4				
Hex. graphitic–C_3N_4	C(1)	0.3505	0.1753	0
a=b=4.7363 Å, c=6.4211 Å	C(2)	0.0184	0.5092	$\frac{1}{2}$
$P\overline{6}m2$ [187], Z=2	N(1)	0	0	0
E_{coh}= -65.322 eV/C_3N_4	N(2)	$\frac{2}{3}$	$\frac{1}{3}$	$\frac{1}{2}$
	N(3)	0.1704	0.3408	$\frac{1}{2}$
	N(4)	0.5037	0.4963	0
α–C_3N_4	C(1)	0.5168	0.0809	0.2007
a=b=6.4333 Å, c=4.6821 Å	C(2)	0.1656	0.2547	0.9909
$P3_1c$ [159], Z=4	N(1)	0	0	0
E_{coh}= -65.285 eV/C_3N_4	N(2)	$\frac{1}{3}$	$\frac{2}{3}$	0.6277
K_0= 419.6 GPa	N(3)	0.3470	0.9509	0.9705
	N(4)	0.3148	0.3185	0.2423
β–C_3N_4	C(1)	0.7729	0.1783	$\frac{1}{4}$
a=b=6.3708 Å, c=2.3924 Å	N(1)	$\frac{1}{3}$	$\frac{2}{3}$	$\frac{3}{4}$
$P6_3/m$ [XXX], Z=2	N(2)	0.0329	0.3302	$\frac{1}{4}$
E_{coh}= -65.064 eV/C_3N_4				
K_0= 443.5GPa				
cubic–C_3N_4	C(1)	$\frac{7}{8}$	0	$\frac{1}{4}$
a=5.3810 Å	N(1)	0.2840	0.2840	0.2840
$I\overline{4}3d$ [220], Z=4				
E_{coh}= -64.053 eV/C_3N_4				
K_0= 485.93 GPa				
defect–zincblende–C_3N_4	C(1)	$\frac{1}{2}$	$\frac{1}{2}$	0
a=3.4097 Å	N(1)	0.2551	0.2551	0.2551
$P\overline{4}3m$ [XXX], Z=1				
E_{coh}= -63.829 eV/C_3N_4				
K_0= 426.0 GPa				

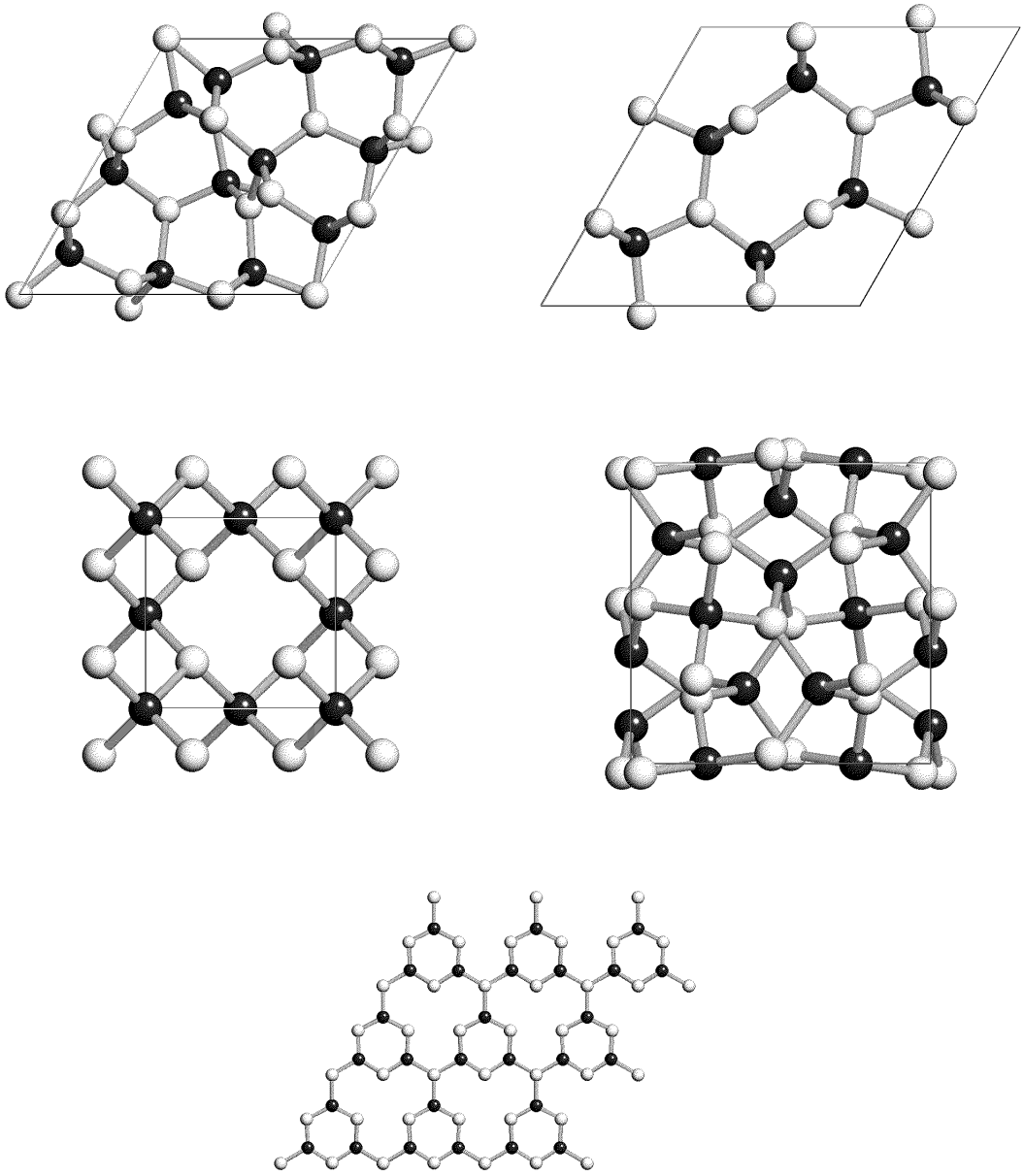

Figure 3.1: Representations of the (a) α–C_3N_4, (b) β–C_3N_4, (c) defect–zincblende-C_3N_4, (d) cubic–C_3N_4 crystal structures and (g) a single layer of graphitic C_3N_4.

3.2 Methodology

In an examination of the energetics and physical properties of these phases of carbon nitride, first-principles electronic structure calculations were completed using density-functional techniques within both the local density approximation (LDA) and the generalized gradient approximation (GGA) to electron exchange and correlation. A preconditioned conjugate-gradient method was used to minimize the electronic degrees of freedom.[158] The electronic wave functions were expanded in a plane-wave basis set with periodic boundary conditions. These calculations were completed using pseudopotentials constructed within the Vanderbilt "ultrasoft" formalism.[219] For each structure, the total energy was calculated over a wide range of unit cell volumes. At a given volume, the positions of the atoms were determined by minimizing the forces on the atoms whereas the unit cell edge lengths were found by equalizing the stresses on the cell. The structural parameters were considered to be fully relaxed when the forces on the atoms were less that 0.001 eV/Åand the components of the stress tensor were less than 0.001 eV/Å^3. The resulting energies were fit to a fourth–order Birch[11] equation of state for calculating the pressure, bulk modulus (K_0) and pressure derivative of the bulk modulus (K_0') (see above).

In order to estimate with a high degree of confidence the energy differences between the structure types, a convergence level of 1 meV/atom was assumed in the calculations. The number of special k points for the Brillouin zone integration was increased until the total energies had converged to below 1 meV/atom. Calculations were also completed at various kinetic energy cutoffs. It was determined that a cutoff of approximately 400 eV was required for a satisfactory convergence of the structural parameters and elastic properties.

3.3 Results

Assuming that a low-energy carbon nitride structure with a high bulk modulus must have carbon four–coordinated with nitrogen and nitrogen three–coordinated with carbon, we have identified several prototype structures. Our methodology is to consider chemical systems with similar bonding topology and to locate dense structures within these systems. Using first-principles pseudopotential total energy calculations[158], we examined a series of C_3N_4 polymorphs to determine their energetics, structure, and physical properties including zero-pressure bulk modulus (K_0), atomic density and band gap.

The β–C_3N_4 structure can be derived from the β–Si_3N_4 structure by replacing the Si atoms in the latter by C. This resulting structure is isostructural with that of phenacite (Be_2SiO_4), and consists of four–coordinate carbon linked by three coordinate N atoms into a network of 3-, 4- and 6-membered rings of CN_4 tetrahedra (Fig. la). The unit cell contains 14 atoms and has $P6_3/m$ symmetry. The α–C_3N_4 structure can be described as an $\cdots$ABAB$\cdots$ stacking sequence of alternating layers of β–C_3N_4 and its mirror image. The unit cell contains 28 atoms and has $P3_1c$ symmetry (Fig. 1b). When calculations were completed on α–C_3N_4 under $P3$ symmetry, no changes were encountered in the atomic coordinates. Two graphitic forms of carbon nitride have also been considered. These structures are constructed from the defect–graphitic layer shown in Figure 3.1. The rhombohedral polymorph consists of an $\cdots$ABCABC$\cdots$ stacking of the planar structure. Its primitive unit cell contains 7 atoms and exhibits $R3m$ symmetry. The hexagonal–graphitic polymorph is constructed of $\cdots$ABABAB$\cdots$ stacking of the defect–graphitic layers. Its unit cell contains 14 atoms and posesses $P\overline{6}m2$ symmetry. Another candidate suggested by this analysis is the defect–zincblende structure type, a structure-type previously studied by Liu *et al.*.[116] It exhibits $P\overline{4}3m$ symmetry and contains seven atoms in the unit cell. We also searched for possible candidate structures in the Zn_2SiO_4 system, because the zero-pressure willemite structure

is isostructural with that of phenacite. In a study of high-pressure transformations in zinc silicates, Syono *et al.* found that willemite transforms at 3 GPa at 1400°C to a tetragonal phase with the same type of 3–, 4–bonding topology, a phase that can be quenched to ambient conditions.[190] This structure exhibits $I\overline{4}2d$ symmetry and has 28 atoms in the unit cell. The cubic–C_3N_4 material studied in this work is based on this high-pressure $I\overline{4}2d$–Zn_2SiO_4 structure.[129] When C is substituted for Zn and Si, and N is substituted for O, the structure was found to relax in a calculation to cubic $I\overline{4}3m$ symmetry (Fig. 1e). All of the dense structures possess similar C–N bond lengths, intertetrahedral C–N–C and intratetrahedral N–C–N bond angles. As shown in Fig. /refc3n4ev, α–C_3N_4 is predicted to have a lower energy than β–C_3N_4 at all of the volumes studied. The graphitic–C_3N_4 structure is predicted to have a slightly lower energy than α–C_3N_4. This result agrees qualitatively with earlier calculations comparing the energetics of planar–C_3N_4 to those of β–C_3N_4.[119, 154] The graphitic phase is a promising precursor for the high–pressure synthesis of C_3N_4 compounds.

At zero-pressure, the cubic–C_3N_4 structure is higher in energy than both α– and β–C_3N_4, but as the pressure is increased, it becomes the thermodynamically favored phase. The transition pressure from α– to cubic–C_3N_4 is predicted by our calculations to be approximately 68 GPa. The transition pressure from graphitic–C_3N_4 to cubic–C_3N_4 is predicted to be approximately 12 GPa, which can be easily attained using large volume presses. For the cubic–C_3N_4 structure, the calculated zero-pressure bulk modulus, K_0 is 485 GPa, which is greater than the experimental K_0 of diamond (443 GPa). This is a very significant result, as it is the first prediction of a material with a bulk modulus larger than diamond.

The widespread interest in carbon nitrides also arises from their predicted wide band gap and high atomic density. The high–pressure cubic-C_3N_4 phase is predicted to have a band gap of 2.90 eV. α—C_3N_4 has a band gap of 3.85 eV, and β–C_3N_4 has a band gap of 3.25 eV. Because LDA typically underestimates the experimental band gap by 15-20%, the actual

band gaps of these materials, if they can be synthesized, should be higher. All of these phases except the graphitic-types have predicted atomic densities approaching that of diamond (experimental result: 0.2950 mol- atoms/cm^3, LDA result: 0.3007 mol-atoms/cm^3). We find the atomic density of cubic-C_3N_4 to be 0.2985 mol-atoms/cm^3. On the basis of its high atomic density and bonding topology, cubic-C_3N_4 should be an excellent thermal conductor. Most experimental studies of carbon–nitrides have been carried out at ambient or low–pressure conditions. Our results indicate the importance of high-pressure synthesis in the search for new carbon nitrides .

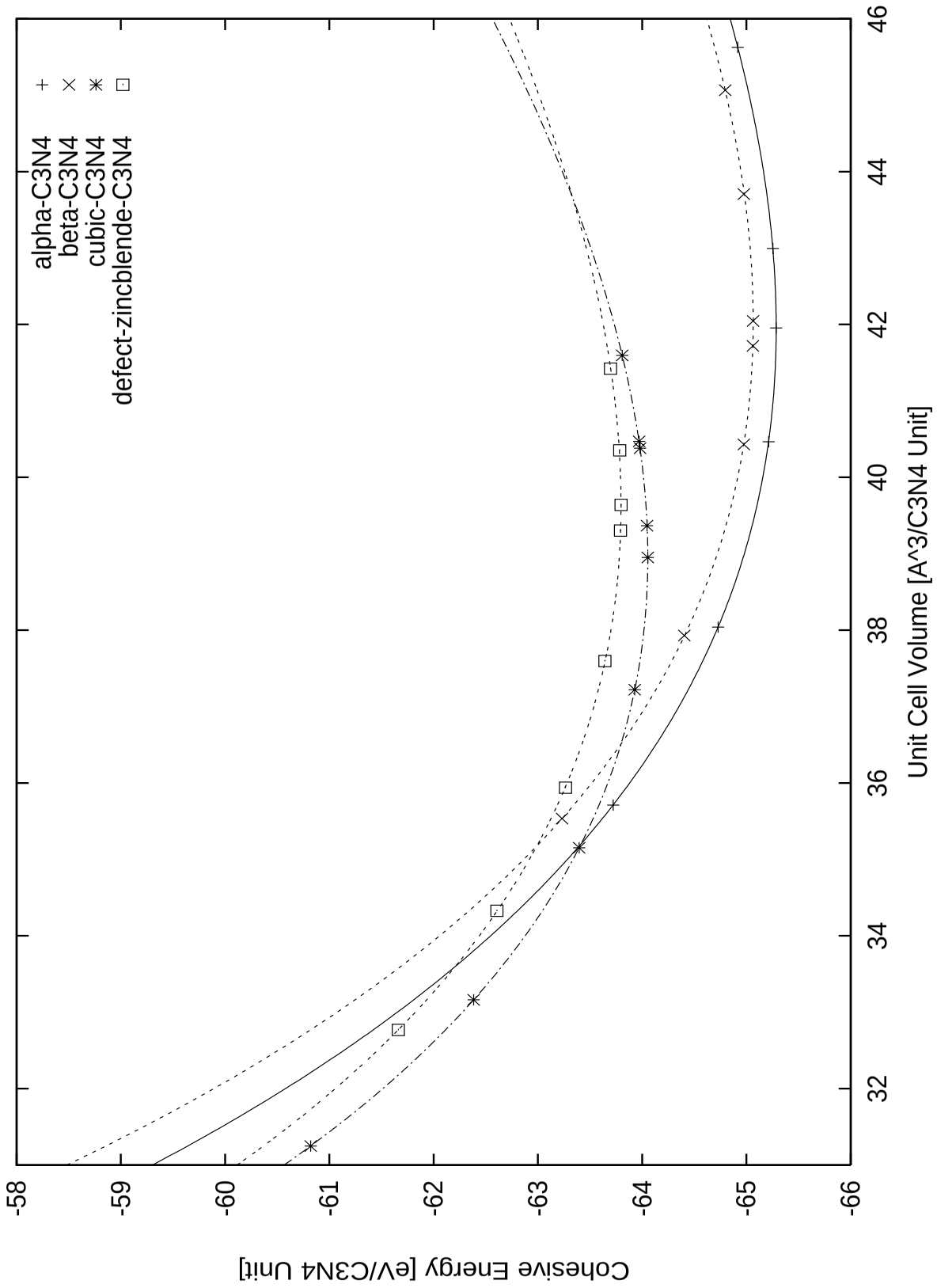

Figure 3.2: Cohesive energy vs. unit cell volume for several polymorphs of C_3N_4.

3.4 Discussion

3.4.1 Energetics and Structure: The effect of lone-pair interactions

Recently, the energetic stability of β–C_3N_4 has been questioned from both chemical[3, 60, 78, 86, 201] and thermodynamical[3, 183] grounds. The primary chemical concerns are the presence of trigonal planar NC_3 groups and short nitrogen–nitrogen distances. The argument against planar NC_3 groups is related to observations that in several molecular structures NSi_3 groups are planar while NC_3 groups are pyramidal.[86] As the β–Si_3N_4 structure contains planar NSi_3 groups, the isostructural β–C_3N_4 also contains planar NC_3 groups. It has been suggested that there is sufficient N($2p_z$)$\rightarrow$ Si($3d$) π–bonding to stabilize the planar configuration of Si about the N atom.[34, 169] As carbon has no low–energy d orbitals, the σ–bonding alone determines the pyramidal configuration.[34] For $N(CH_3)_3$, the energy barrier to planarity has been calculated to be 7.9 kcal/mole (HF,6-31G** basis).[60] This result led Guo and Goddard to examine the energetic feasibility of the β–C_3N_4 structure using an interatomic potential parameterized from *ab initio* studies on the $N_4(CH_2)_6$ molecule.[60] They found when the symmetry of β–C_3N_4 is lowered to $P3$, the planar–NC_3 groups buckle into a pyramidal configuration. They concluded that previous studies had improperly constrained the NC_3 groups to be planar. However, when their buckled β–C_3N_4 structure is optimized, using first-principles methods, we find that the CN_3 groups adopt a planar configuration.[197] It appears that the buckling of the CN_3 groups in their study is an artifact of their molecular–based potential. However, CN_3 groups are not universally pyramidal in molecules as observed by Tossell who found that planar groups are adopted in larger molecules like $C_6N_5H_{15}$ and $C9n_9H_{21}$. [203]

The argument against the short N–N distances is more serious and is based upon the destabilizing effect of N–N "lone pair" interactions. In β–Si_3N_4, the N–N distances are 2.91 $\mathring{A}$ and 3.18 $\mathring{A}$ for the planar nitrogens. In β–C_3N_4, these distances are found to be 2.35 Åand 2.40 Å. This is of significant concern, as the energetics of C_3N_4 structures appear to be primarily determined by their ability to minimize these interactions.[200] A structure that minimizes these interactions should be favored energetically. The α–C_3N_4 phase is lower in energy than β–C_3N_4 as it accomodates these interactions more effectively and possesses fewer non-planar NC_3 groups. Figure 3.3 shows the electronic total density of states for the carbon nitride polymorphs. Nitrogen nonbonding electronic states should occupy the highest occupied valence band. This is analogous to the highest occupied molecular orbital (HOMO). The lowest energy structure, α–C_3N_4, has the fewest number of high-energy states at the top of the valence band. The β–C_3N_4 structure is higher in energy, and has more states at the top of valence band. The defect–zincblende structure is significantly higher in energy as the several nonbonding pairs are directed towards each other at the center.

Hughbanks and Tian proposed an elegant solution to the N–N interaction problem by constructing a structural model in which the planar nitrogens are replaced with carbon.[78] By doubling the cell along **c**, these carbons can be displaced to become tetrahedrally bonded with each other. This solution leads to a stochiometry of C_4N_3, and has the advantage that the atoms occupying these sites attract, rather than repel one another. While this does induce added strain into the structure, removing the N–N lone pair interactions lowers the energy of the structure below that of any of the C_3N_4 compounds. This structure is also lower in energy than if one were to replace the planar N in β–C_3N_4 with C and to leave the C in three-fold coordination.

Table 3.2: Calculated structural zero–pressure structural parameters for the carbon nitride structures discussed in the text.

Structure	Atom	x	y	z
C_4N_3	C(1)	$\frac{2}{3}$	$\frac{1}{3}$	0.4584
a=b=6.535 Å, c=4.677 Å	C(2)	$\frac{2}{3}$	$\frac{1}{3}$	0.7911
$P3/overline3$ [147], Z=4	C(3)	0.8238	0.2214	0.3806
K_0= 392.6 GPa	C(4)	0.8198	0.2186	0.8697
	N(1)	0.9549	0.2989	0.1230
	N(2)	0.9686	0.2822	0.6278

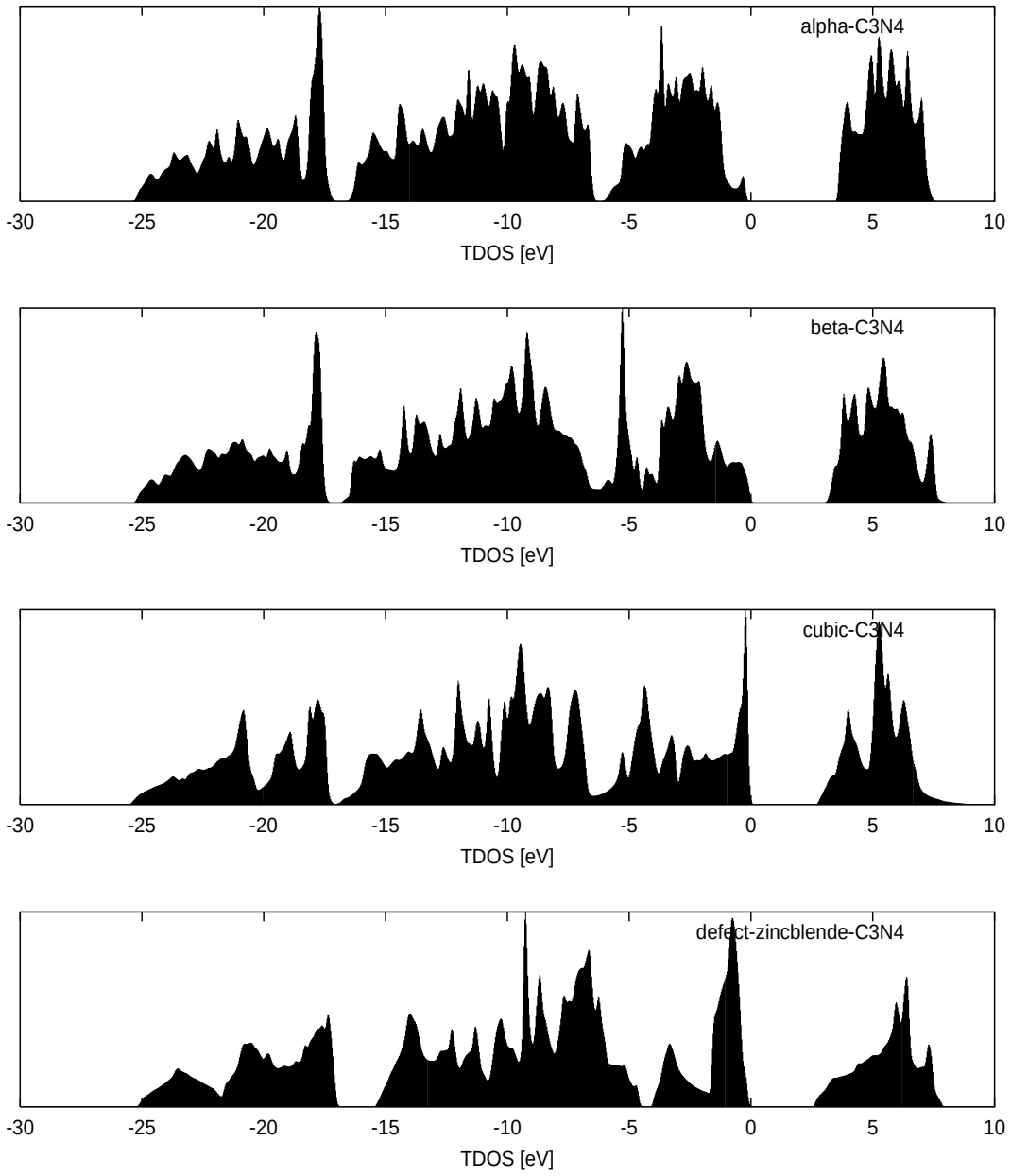

Figure 3.3: Total electronic density of states for several of the carbon nitride polymorphs discussed in the text.

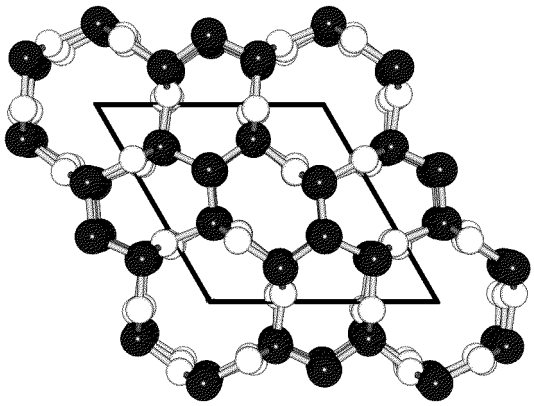

Figure 3.4: Representation of the C_4N_3 structure described in the text. The dark atoms represent the carbon atoms, while the light atoms represent the nitrogen atoms.

3.4.2 The Role of Pressure in the Synthesis of Carbon Nitride

Earlier in this chapter, it was described how α–C_3N_4 and cubic-C_3N_4 could be synthesized from graphitic–C_3N_4 at pressures achievable in the diamond-anvil cell, possibly at pressures achievable in industrial presses. An issue that was not discussed is the enthalpic stability of C_3N_4 relative to a mixture of diamond and ϵ–N_2 as a function of pressure. This was recently examined by Badding and Nesting assuming a combination theoretical and experimental values for their thermodynamic calculation.[3] They found that both β–C_3N_4 and the C_4N_3 phases suggested by Hughbanks and Tian become enthalpically favored at pressures in the vicinity of 80–100 GPa. We calculated the equation of state for α–C_3N_4, cubic-C_3N_4, C_4N_3, diamond, and ϵ–N_2 using first-principles methods. A difficulty exists in comparing the total energies of structures with different types of bonding and density. It is recognized that mean-field approximations like the LDA electronic correlation differently for different densities. Recent Diffusion Monte Carlo (DMC) studies by Mitas *et al.* quantify the errors between the LDA total energy and the DMC total energy for different phases of N_2.[138] They show that these errors are greatest for the atom, and decrease as one goes to the dimer, the molecular crystal and then to a hypothetical dense crystalline phase of N_2. At high enough densities, these errors are minimized, as the LDA is parameterized from the DMC result.[20] We correct our LDA total energy for ϵ–N2 and diamond using recent DMC results[138, 139] As the densities and bonding in the carbon nitrides are similar to diamond, we offset the total energies of α–C_3N_4, cubic–C_3N_4, and C_4N_3 by the DMC diamond result.[139] As seen in Figure 3.5 C_4N_3 is favorable to C_3N_4 at ambient pressures, but the synthesis of cubic–C_3N_4 is favored at pressures above 80 GPa.

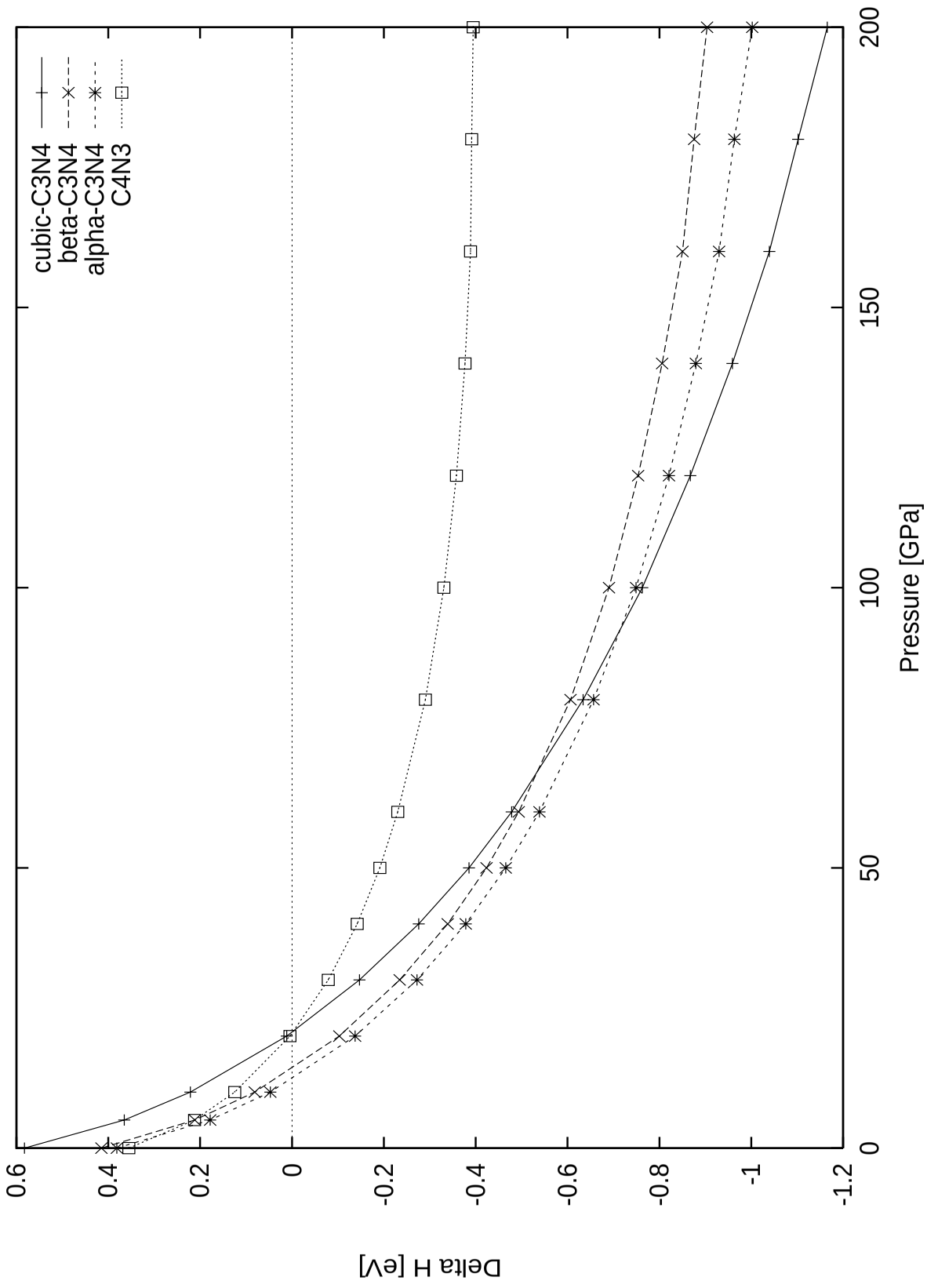

Figure 3.5: ΔH of various carbon nitrides vs. pressure

3.4.3 Predicting the Hardness of Carbon Nitrides

The motivation behind the search for carbon nitrides has been based upon the prediction that their hardness should rival or even exceed that of diamond because of their high bulk moduli[23, 116, 118, 119, 154, 166, 197, 230] and the premise that materials with high bulk moduli are necessarily hard. [26, 53, 110, 116, 163, 189, 229] In this chapter we have identified a crystal structure (cubic–C_3N_4) with a predicted bulk modulus of 485 GPa This is the first prediction of a material with a bulk modulus that exceeds that of diamond. Based upon the assumption that the bulk modulus is an excellent predictor of hardness, this material should be harder than diamond. However, we have shown in Chapter 2 that the shear modulus is a significantly better predictor of the hardness of a material. In order to better determine the potenital hardness of cubic–C_3N_4 and various other carbon nitrides, we need to undertake a calculation of the elastic constants for various phases of carbon nitride and determine their shear moduli.

A Methodology for Determining the Elastic Constants of a Cubic Crystal

We can determine the elastic constants of a cubic crystal by considering the relationships between the elastic constants and the strain energy of a crystal. If we strain the lattice by distorting the primitive basis vectors and allowing the positions of the atoms to relax in order to minimize the total energy, the elastic constants (c_{ij}) of the crystal can be obtained. Considering the strain tensor with six independent components:

$$\epsilon = \begin{pmatrix} e_1 & e_6/2 & e_5/2 \\ e_6/2 & e_2 & e_4/2 \\ e_5/2 & e_4/2 & e_3 \end{pmatrix} \tag{3.2}$$

The total energy changes by an amount

$$E(e_i) = E_0 - P(V)\Delta V + V\sum_{i=1}^{6}\sum_{j=1}^{6} c_{ij}e_ie_j/2 + O[e_i^3] \tag{3.3}$$

where V is the volume of the undistorted lattice, $P(V)$ is the pressure of the undistorted lattice at volume V, ΔV the change in volume due to the applied strain, and O$[e_i^3]$ indicates that the cubic and higher srain terms are neglected from the polymomial expansion. While there are 36 elastic constants in Formula 3.3, only 21 of these elastic constants are independent. In the case of a crystal with cubic symmetry, there are only three independent elastic constants: c_{11}, c_{12}, and c_{44}. The bulk modulus of a cubic crystal can be related to these elastic constants by:

$$B = (c_{11} + 2c_{12})/3 \tag{3.4}$$

The remaining elastic constants can be calculated by straining the crystal in certain directions and calculating the resulting change in internal energy. We can calculate the tetragonal shear modulus (c_{11}-c_{12}) with a volume–conserving orthorhombic strain.

$$\begin{aligned} e_1 &= -e_2 = x \\ e_3 &= x^2/(1-x^2) \\ e_4 &= e_5 = e_6 = 0 \end{aligned} \tag{3.5}$$

This strain will change the total energy by the amount:

$$\Delta E(x) = \Delta E(-x) = V(c_{11} - c_{12})x^2 + O[x^4] \tag{3.6}$$

We can now calculate the c_{44} elastic constant using a volume–conserving monoclinic strain.

$$\begin{aligned} e_6 &= x \\ e_3 &= x^2/(4-x^2) \\ e_1 = e_2 &= e_4 = e_5 = 0 \end{aligned} \tag{3.7}$$

The total energy is a function of the strain x:

$$\Delta E(x) = \Delta E(-x) = V c_{44} x^2/2 + O[x^4] \tag{3.8}$$

These single–crystal elastic constants can be used to compute upper and lower bounds on the polycrystalline aggregate shear modulus using the bounds derived by Hashin and Shtrikman.[71] For the cubic case, the shear modulus is bounded by

$$G_1 = \frac{7c_{11}^3 - 12c_{11}^2c_{12} + 61c_{11}^2c_{44} - 65c_{11}c_{12}c_{44} + 3c_{11}c_{12}^2 + 4c_{12}^2c_{44} + 2c_{12}^3}{59c_{11}^2 - 55c_{11}c_{12} + 32c_{11}c_{44} - 8c_{12}c_{44} - 4c_{12}^2} \tag{3.9}$$

$$G_2 = \frac{c_{44}(47c_{11}c_{44} - 20c_{12}c_{44} + 24c_{44}^2 + 8c_{11}^2 + 8c_{11}c_{12} - 16c_{12}^2)}{37c_{11}c_{44} + 20c_{12}c_{44} + 64c_{44}^2 + 3c_{11}^2 + 3c_{11}c_{12} - 6c_{12}^2} \tag{3.10}$$

If we define the Shtrikman modulus as the smaller of G_1 and G_2 and the Hashin modulus as the larger, the shear modulus is bounded by

$$G_s < G < G_h \tag{3.11}$$

Finally, the crystal is mechanically stable if it meets the Born stability criteria. For a cubic crystal, these are:

$$\begin{aligned} B = (c_{11} + 2c_{12})/3 > 0 \\ c_{11} - c_{12} > 0 \\ c_{44} > 0 \end{aligned} \tag{3.12}$$

Calculating the Elastic Constants for cubic–C_3N_4

Using the methodology outlined above, we can now determine the elastic constants for cubic–C_3N_4. The energies calculated in response to the volume–conserving orthorhombic strains defined by Formula 3.5 are listed in Table 3.3. These values are used to determine the (c_{11}-c_{12}) shear modulus using the relationship put forward in Formula 3.6. Undertaking a linear least–squares refinement, we find that the (c_{11}-c_{12}) shear modulus is 562.9 GPa. Since we have previously determined K_0= 485.9 GPa, we can use the relationship in Equation 3.4 to find that c_{11}= 861.2 GPa and c12= 298.3 GPa. To calculate c_{44}, we deform the unit cell using the volume–conserving monoclinic strains defined by Formula 3.7 and obtain the calculated energies listed in Table 3.4 Undertaking a least–squares fit of the data using the relationship in Formula 3.8, we find that c_{44}= 513.8 GPa. These elastic constants yield an average aggregate shear modulus of 404 GPa and the crystal meets the Born criteria for mechanical stability. The results of similar calculations for the defect–zincblende-C_3N_4 and β–C_3N_4 structures are given in Table 3.5. These values for the shear moduli of various C_3N_4 polymorphs are significantly less than that of diamond (535 GPa). Based upon the relationship between the shear modulus and hardness, it is unlikely that these structures will be harder than diamond.

Table 3.3: Results of LDA calculations to determine the (c_{11}-c_{12}) shear modulus of cubic–C_3N_4 using a [444] MP–grid at a kinetic energy cutoff of 347.853 eV.

x	E [eV]	Δ E [eV]	Vx^2 [Å^3]
0.000	-256.218097	0	0
0.010	-256.157212	0.060885	0.015581
0.020	-255.993707	0.224390	0.062323
0.030	-255.717912	0.500185	0.140227
0.040	-255.336750	0.881347	0.249292

Table 3.4: Results of LDA calculations to determine the c_{44} shear modulus of cubic–C_3N_4 using a [444] MP–grid at a kinetic energy cutoff of 347.853 eV.

x	E [eV]	Δ E [eV]	$Vx^2/2$ [Å^3]
0.000	-256.218097	0	0
0.020	-256.114692	0.103405	0.031162
0.030	-255.984812	0.233285	0.070113
0.040	-255.811253	0.406844	0.124646
0.050	-255.585354	0.632743	0.194760
0.060	-255.313448	0.904649	0.280454

Table 3.5: Bulk and shear moduli for several of the carbon nitrides considered.

Structure	Bulk Modulus [GPa]	Shear Modulus [GPa]
β–C_3N_4	443.5	320
cubic–C_3N_4	486.3	404
defect–zincblende–C_3N_4	426.0	405

3.5 Conclusions

We have used first–principles total-energy calculations to examine the physical properties 0f a set of hypothetical C_3N_4 structures. We find that the graphitic phase has the lowest energy of any phase considered and that α–C_3N_4 has a lower energy than β–C_3N_4. We examined a cubic form of C_3N_4 with a zero-pressure bulk modulus exceeding that of diamond. Like diamond, this new phase could potentially be synthesized by subjecting the graphitic phase to high temperature and pressure, and quenching it to ambient pressure for use as a superhard material We have used a robust set of hardness data to show that the shear modulus is a better predictor of hardness than the bulk modulus. This has implications for the predictions of hardness for carbon nitride, as the shear modulus of defect–zinclende-, cubic- and β–C_3N_4 are only 60–75%that of diamond. While it appears that C_3N_4 should be a superhard material, it seems unlikely that it will be harder than cubic-BN, let alone diamond. However, these materials still possess several valuable properties such as high bulk modulus, high atomic density, and a wide band gap.

Chapter 4

High Pressure Phases of Silica

4.1 Introduction

The behavior of silica under pressure has been of long and continuing interest due to its wide ranging implications in geophysics, materials science, and fundamental physics[76]. Since the discovery of stishovite[184], a dense polymorph of silica with octahedrally–coordinated silicon, there has been significant interest in the possibility of denser phases at high pressure. It has recently been suggested that stishovite is the hardest known oxide, possessing a Vickers hardness of 33 GPa.[110] Furthermore, it has also been suggested that post–stishovite phases of silica may exist that are potentially harder than diamond.[1] Stishovite undergoes a displacive phase transformation to the $CaCl_2$ structure type at pressures above 50 GPa[94]. This result is in excellent agreement with first–principles predictions of this transformation prior to its experimental determination. The behavior of silica at higher pressures is not clear, as new phases have been observed from both static and dynamic compression of amorphous silica[124, 40], α–cristobalite[214, 227], and α–quartz[45, 95], but the analysis of much of this data is difficult and the interpretations contradictory. Several experimental studies

have yielded different results at similar pressure and temperature conditions. Recently, a new post–stishovite phase designated $Pnc2$–type silica has been proposed theoretically[10] and reportedly synthesized at high pressure[40]. There is also experimental and theoretical evidence for the possibility of other post–stishovite phases including those having the Fe_2N[124], α–PbO_2[45], $I2/a$[210], baddelyite, fluorite, and $Pa3$[205, 131] structures. Hence, it remains unclear what stable or metastable phases of silica exist at high pressures and what the physical properties, such as hardness, of these phases are.

We have undertaken a study to determine the phases of silica that are stable at high pressures and their physical properties. In the study, a method was developed for generating a large number of promising structure types. First–principles electronic structure calculations were completed on the most favorable structures in an exploration of the their energetics and the physical properties. For a discussion of these calculations employeed in this study, see Chater 3.

4.2 Computational Details

First–principles pseudopotential plane–wave total-energy calculations within the local density approximation (LDA) to electronic exchange and correlation were performed on the model structures[158]. This method accurately reproduces many of the physical properties of silica[76, 210, 89, 90]. Vanderbilt ultrasoft pseudopotentials[219] were generated for silicon and oxygen. The electronic degrees of freedom were minimized using a preconditioned conjugate–gradient method and both the ionic positions and cell parameters were fully optimized at all volumes. Due to extremely small energy differences between structures, a convergence of 0.001 eV/SiO_2 unit was employed for energy differences with respect to kinetic energy cutoff and for the total energy with respect to Brillouin zone integration. While

a kinetic energy cutoff of 400 eV was found sufficient to converge the structures a cutoff of 750 ev was needed to converge the energy differences. Monkhorst–Pack special k-point grids were used for the Brillouin–zone integration. In addition, we calculated the equations of state of stishovite and $CaCl_2$–type silica using the generalized gradient approximation (GGA) proposed by Perdew *et al*[160]. We find the LDA provides a significantly better prediction of the experimental equations of state[76].

4.3 Generation of New Structure Types

The structure types of silica with octahedrally–coordinated silicon can be visualized and understood in a simple manner. This allows us to methodically generate a series of new structures. Many crystal structures can be visualized in terms of close–packed arrays of anions or cations. These arrays can be described as either hexagonal (*hcp*) or cubic (*ccp*), or mixtures of the two stacking sequences. For each ion in the array, there are two available tetrahedral interstices and one available octahedral interstice. For example, the high pressure silica polymorph, stishovite, the thermodynamically stable form above 7 GPa[76, 184] possesses the rutile structure and can be described as a distorted *hcp* array of oxygen ions with one-half of the available octahedral interstices occupied by silicon ions. This results in the formation of straight chains of edge–sharing SiO_6 octahedra which are corner linked between $\cdots$ABAB$\cdots$ layers to form a three dimensional network (similar to $CaCl_2$ as shown in Fig. 1a). The α–PbO_2 structure is observed as a post–rutile phase in a number of analogous systems, and can also be described in terms of a *hcp* packing of oxide anions. However, in this case the silicon ions are arranged in such a way as to generate 2x2 zigzag chains of edge–sharing octahedra (Fig 1e). These structures can also be described as *deconstructions* of their MX superstructures[224], which for *hcp* and *ccp* are the NiAs and NaCl structure

types, respectively. In both structures, the cations occupy all of the octahedral sites between the close–packed anion layers. The removal of one-half of the M ions from the NiAs structure results in the generation of the rutile and α–PbO_2 structures. Novel framework structures of MX_6 octahedra can be generated by constructing NiAs– or NaCl–type supercells, or combinations of these stackings and methodically removing one-half of the metal ions according to simple rules[224].

We used this method of *deconstruction* to derive new octahedral framework structures. After generating a new structure, a supercell is constructed and allowed within the constraints of $P1$ symmetry using an enthalpy minimization method where the energies are obtained using the BKS interatomic potential[218]. This potential has been shown to accurately model the equations of state of both quartz and stishovite[5, 208]. In the derivation, these structures are compressed to a pressure of 100 GPa and checked for both mechanical and dynamical stability. Structures with competitive enthalpies ($H = E + PV$) are then optimized using first–principles calculations, and their equations of state obtained.

4.4 Results and Discussion

4.4.1 Sequence of High Pressure Phase Transitions

In contrast to previous work on dense silica in which only a few specific structures were examined[76, 10, 210, 89, 90], we have generated several hundred thousand structures during the course of this study. We find the most favorable consist of edge–sharing octahedral chains with varying degrees of kinking. The density of these structures correlates directly with the number of kinks along the chains. Of these octahedra structures, stishovite (straight chains) is the least dense, while α-PbO_2 type (with the most possible kinks in for a 2x2 zigzag

chains) is the densest, with an essentially infinite number of intermediate structures. As archetypes, we discuss the results for structures with 4x4, 3x3, and 3x2 kinked octahedral chains in ($\cdots$ABAB$\cdots$) stacking, and compare them to previously examined structures and experimental diffraction data.

In agreement with previous work[94, 89], these calculations find stishovite to be the most stable phase between pressures of 20? and 55 GPa, whereupon it undergoes a displacive phase transition to the $CaCl_2$ structure type. The layers of oxygen anions adopt what appears to be a closer packing than is allowed by the rutile structure. The concept of eutaxy[151] states that structures adopt these packings not because ions behave as "hard spheres", but because these arrays offer effective geometric solutions to maximize the anion–anion and cation–cation separations while maintaining near ideal cation–anion bond lengths. The favorability of these structures at high pressure is determined by a delicate balance between maximizing cation–anion attractions, minimizing anion–anion and cation–cation repulsions, while simultaneously maximizing the density.

Our predicted sequence of high–pressure structures is as follows (see Fig. 4.2). At 85 GPa, the α–PbO_2–type becomes the stable phase. It is denser than the $CaCl_2$–type and allows greater oxygen–oxygen separation. The $I2/a$–type phase proposed by Tse *et al.*[210], is not favored at high pressure due to its low density relative to stishovite. We also find that silica in the baddelyite structure is not energetically competitive with the structures discussed here, and it is mechanically unstable below 100 GPa. Above 95 GPa, the kinked phases presented here are all preferred relative to the $CaCl_2$–type structure. The 4x4 structure type (Fig. 1b) has been reported for an epitaxially modified form of SnO_2[143]. The 3x3 structure type (Fig. 1c) is adopted by α–$NaTiF_4$[152]. The 3x2 structure type (Fig. 1d) is previously unreported and found to be only slightly higher in enthalpy than the 2x2 α–PbO_2 type. As the intermediate kinked phases are both structurally similar to and enthalpically competitive

with the $CaCl_2$ and α–PbO_2 structures, there is considerable possibility that they may exist as metastable phases at high pressure.

At pressures above 205 GPa, the $Pa3$–type structure (Figure 4.3) is indicated to be the stable phase. This structure type was first observed experimentally following the compression of rutile–type PdF_2[204]. The high–pressure $Pa3$–phase was first proposed to be a possible post–stishovite phase by Tressaud and Demazeau.[205] It has since been proposed that this structure type is adopted as a post–rutile phase for metal dioxides instead of the fluorite structure[63]. Constructed of corner–sharing SiO_6 octahedra, this structure allows increased anion–anion and cation–cation separation as compared to the previous close–packed phases. The higher pressure $Pa3$ phase, which has not yet been observed experimentally, was first studied theoretically by Matsui and Kawamura[131] in molecular dynamics simulations, and subsequently studied using first-principles methods by Parks, Terakura, and Matsui.[155]

Table 4.1: Calculated zero–pressure structural parameters for the structures described in the text.

Structure	Atom	x	y	z
Stishovite	Si(1)	0	0	0
$P4_2/mnm$ [136] Z=2	O(1)	0.3053	0.3053	0
a=4.154Å, b=4.154Å, c=2.667Å				
K_0= 306 GPa K_0'= 4.6				
4x4 SnO_2–type	Si(1)	0	0.0607	$\frac{1}{4}$
$Pbcn$ [60] Z=12	Si(2)	0.9964	0.3573	0.4162
a=4.086Å, b=4.987Å, c=13.488Å	O(1)	0.2910	0.1292	0.0296
K_0= 311 GPa K_0'= 4.0	O(2)	0.7877	0.0882	0.1376
	O(3)	0.2295	0.3330	0.1954
3x3 $NaTiF_4$–type	Si(1)	0	0.7949	$\frac{1}{4}$
$Pbcn$ [60] Z=8	Si(2)	0	$\frac{1}{2}$	0
a=4.067Å, b=4.993Å, c=8.975Å	O(1)	0.7298	0.0233	0.1670
K_0= 317 GPa K_0'= 4.0	O(2)	0.7843	0.7663	0.4177
3x2 $P2_1/c$–type	Si(1)	$\frac{1}{2}$	0	0
$P2_1/a$ [14] Z=6	Si(2)	0.1656	0.5032	0.9657
a=7.619Å, b=4.063Å, c=4.996Å	O(1)	0.0545	0.2327	0.6557
β=118.09°	O(2)	0.7227	0.2286	0.1823
K_0= 320 GPa K_0'=4.0	O(3)	0.3897	0.2149	0.6542
2x2 α–PbO_2–type	Si(1)	0	0.1502	$\frac{1}{4}$
$Pbcn$ [60] Z=4	O(1)	0.2576	0.3870	0.4201
a=4.049Å, b=5.001Å, c=4.468Å				
K_0= 329 GPa K_0'=3.9				
HP-PdF_2–type	Si(1)	0	0	0
$Pa3$ [205] Z=4	O(1)	0.3445	0.3445	0.3445
a=4.422Å				
K_0= 347 GPa K_0'= 4.1				

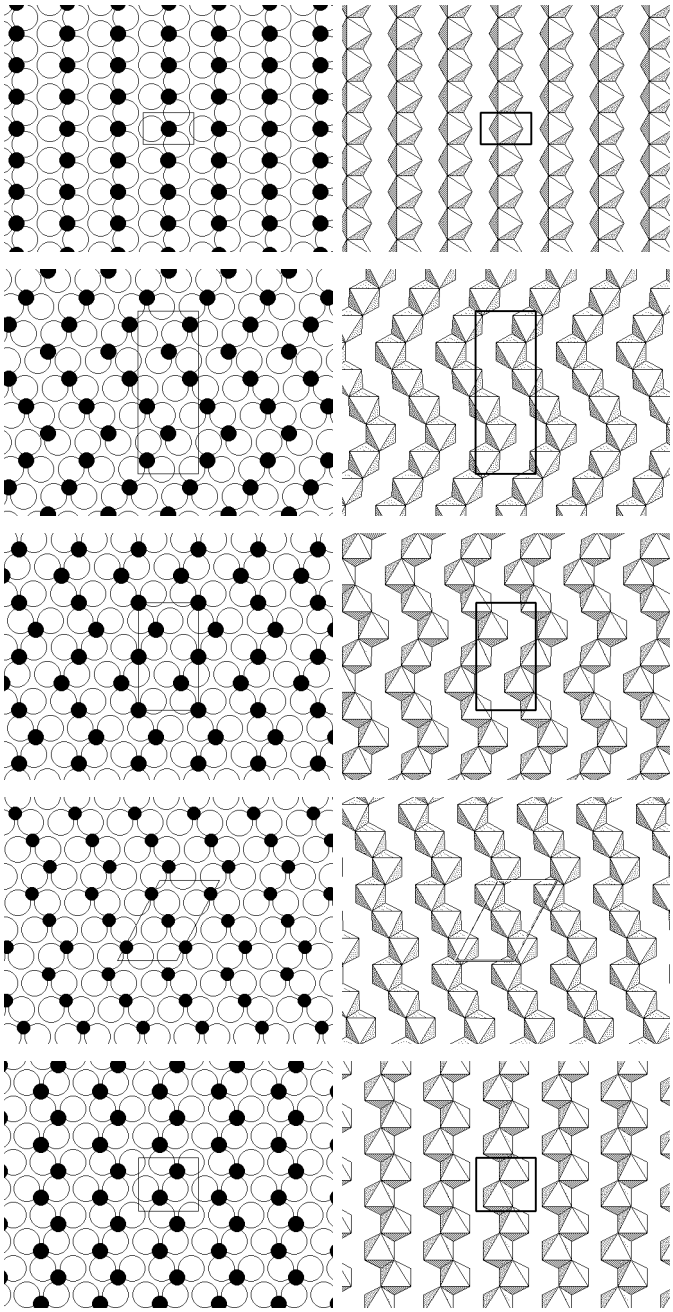

Figure 4.1: Representations of the (1a) $CaCl_2$, (1b) 4X4–SnO_2, (1c) 3X3–$NaTiF_4$, (1d) 3X2 $P2_1/c$, and (1e) α–PbO_2 structure types. The left–hand figures show one layer of the $ABAB...$ stacking of *hcp* oxygen anions (white) with one–half of the octahedral interstices filled with silicon ions (black). The right–hand figures show how these patterns form edge–sharing octahedral chains with various degrees of kinking.

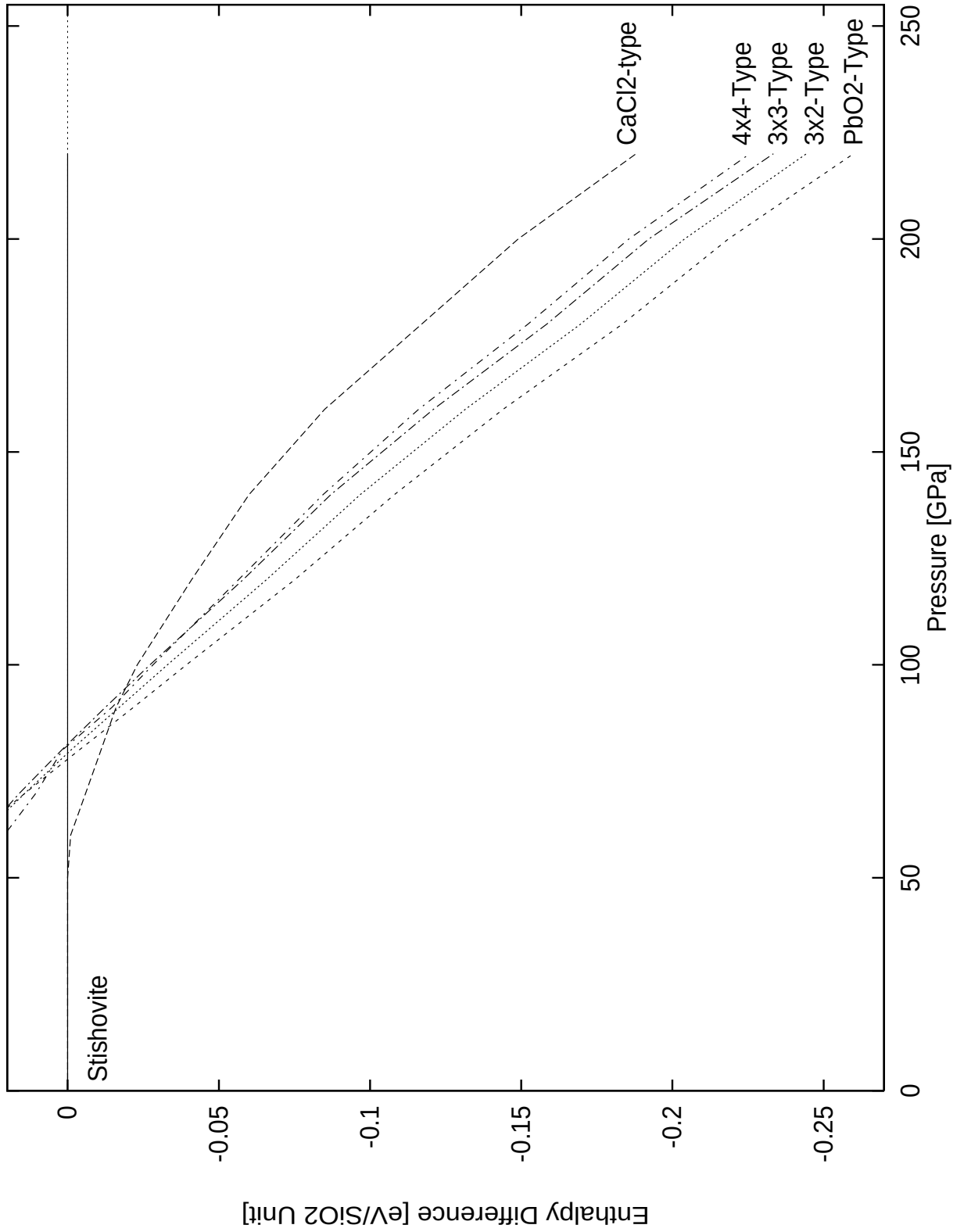

Figure 4.2: Enthalpies of silica structures relative to the enthalpy of stishovite as a function of pressure.

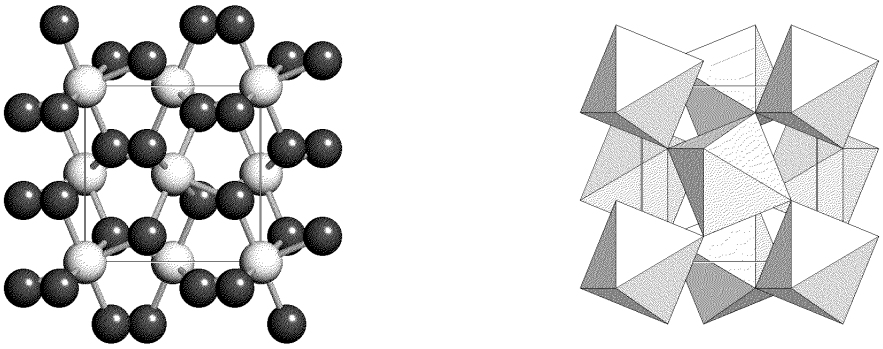

Figure 4.3: Representations of the high–pressure $Pa3$–SiO_2 structure in terms of a ball and stick and a polyhedral models.

4.4.2 A Rexamination of Recent Experimental Data

We now show that these predictions can be used to reinterpret a number of experimental high–pressure results for silica. Recently, Dubrovinsky *et al.*[40] reported the synthesis of a new form of silica by laser–heating amorphous silica at high pressure. They refer to this new as *Pnc*2–type silica based upon a previous theoretical study in which this phase was predicted using interatomic potentials. However, when the *Pnc*2–type structure is reexamined using first–principles calculations, we find it adopts the higher symmetry *Pbcn* space group. A simple cell transformation confirms that this is actually the α–PbO_2 structure type. The transformation matrix between the α–PbO_2 (1) and the *Pnc*2 (2) cells is: $\mathbf{a_1}=\mathbf{b_2}$, $\mathbf{b_1}=\mathbf{c_2}$, $\mathbf{c_1}=\mathbf{a_2}$ and $x_1=-y_2$, $y_1=z_2+0.0136$, $z_1=x_2+\frac{1}{4}$. At any given pressure, the optimized *Pnc*2 and α–PbO_2 structures have the same total energies and simulated diffraction patterns. It is likely that Dubrovinsky *et al.* synthesized the α–PbO_2 phase based upon the good agreement between their experimental and our theoretical diffraction patterns.

German *et al.*[45] have claimed synthesis of α–PbO_2–type silica from the dynamic compression of quartz, but we find poor agreement between their reported and our theoretical diffraction patterns. Very recently, Yamakata and Yagi synthesized a metastable phase from the compression of cristobalite to pressures of ???[227]. Based upon the similarities between these experimental diffraction patterns and those reported for the kinked phases, we believe these experiments resulted in the synthesis of similar metastable close–packed phases, as yet unidentified.

Kingma *et al.*[95] recently reported the synthesis of a dense phase of silica from nonhydrostatic compression of polycrystalline quartz to 213 GPa at room temperature. We find that when the compression of a 18–atom orthorhombic cell of α–quartz above 25 GPa is simulated, using an enthalpy minimization scheme with the BKS interatomic potential[218],

Table 4.2: Comparison of Kingma *et al.* diffraction data to the theoretical diffraction record of the $P2_1/c$–type at a pressure of 173 GPa.

(hkl)	Experimental	$P2_1/c$–type
$(\overline{1}\overline{1}1)$	—	2.82
(011)	2.68	2.69
$(\overline{2}11)$	2.46	2.45
(111)	2.30	2.23
(300)	2.04	2.05
(310)	1.79	1.76
$(\overline{3}\overline{2}2)$	1.36	1.34
(411)	1.19	1.17
	a=6.9(2)Å,b=3.7(2)Å,c=4.7(3)Å β=118.3(2)°	a=6.96Å,b=3.62Å,c=4.57Å β=118.2°

that the structure exhibits a diffusionless transformation into a 3x2–kinked $P2_1/c$ phase. We generated simulated powder diffraction patterns from LDA–derived $P2_1/c$ unit cells as a function of pressure and found a close correspondence between the experimental and theoretical d-spacings (Table II). This good agreement, along with the low enthalpy of the $P2_1/c$ structure suggest that it may have been synthesized as a metastable phase.

Liu *et al*[124] reported the synthesis of the defect–niccolite Fe_2N-phase from laser–heating of silica at high pressure. This corresponds to a dense ordered *hcp* array of oxygen atoms with silicon atoms disordered over the octahedral sites. This is consistent with our finding that there is an essentially infinite number of energetically competitive structures based on dense ordered arrays of oxygen with silicon filling one–half of the available octahedral sites. Liu *et al.* argue that this is a "post–stishovite" phase, but we find that this phase is not enthalpically favored relative to stishovite/$CaCl_2$ at high pressure and ambient temperatures. However, it is likely that this order–disorder phase is actually the thermodynamically

stable phase at high–pressures and temperatures due to the reduction of the free energy by the increase in configurational entropy brought about by disordering the silicon over the octahedral sites.[200]

Finally, it also provides a mechanism for explaining the nature of short– and intermediate–range structure in high–pressure amorphous silica. Our calculations indicate that the high–density amorphous form (e.g. produced on static compression of silica glass[56]) can be described as a dense array of oxygen ions with silicons disordered over the octahedral sites. Hence, the dense amorphous form may contain significant short– and intermediate–range order, as suggested by Primak[165]. These results further suggest that states of order–disorder and crystallinity (ordered domains) can be achieved by heating amorphous silica under pressure, consistent with the results of Liu *et al.*[124]

4.4.3 Predicting the Hardness of High–Pressure Phases of Silica

Léger *et al.* recently claimed that stishovite is the hardest known oxide.[110] They determined that stishovite has a hardness of 33 GPa which they rationalized in terms of its high bulk modulus (K_0=313 GPa). Ahrens recently suggested that post–stishovite phases of silica may exist that are potentially harder than diamond.[1] Ahrens' hypothesis hinges on the assumption that the fluorite form of silica is stable at high pressures and that it is hard because of its high bulk modulus.

While we have shown that the hardness of a crystal is much better correlated with shear modulus than bulk modulus, the stishovite results are not surprising given that it has a high shear modulus (G_0= 220GPa). In order to determine the potential hardness of the post–stishovite phases we calculated the shear moduli of several of the structures discussed above. It is presently intractable to use first–principles calculations to determine the elastic constants

for most of the kinked–phases due to their low symmetry and large unit cells. Instead, the elastic constants have been obtained from calculations using the BKS interatomic potential to obtain the energies. These results suggest that the shear moduli of the α–PbO_2 and related phases are actually slightly less than that of stishovite.

The fluorite structure considered by Ahrens is not mechanically stable at pressures below 100 GPa. Instead, we have considered the $Pa3$–silica phase which is the stable phase above 200 GPa. Using the methodologies outlined in the previous chapter, we find that c_{11}= 674.1 GPa, c12= 183.1 GPa and c_{44}= 228.9 GPa. These elastic constants yield an average aggregate shear modulus of 235.4 GPa. While this value is approximately 10% greater than the shear modulus of diamond, it is far below shear modulus of diamond (G_0= 535 GPa). Therefore, while $Pa3$–silica might be 10% harder than stishovite, it will not be harder than diamond, and the need for pressures above 200 GPa for it's synthesis do not justify its use as a superhard material. Further, whether the fluorite form of silica is harder that than stishovite may be academic given that the calculations completed by Bukowinski indicate that the fluorite structure type of silica is unstable at ambient pressures.[14]

4.5 Conclusions

In summary, we have shown that extensive polymorphism in silica is possible at high pressure, with an essentially infinite number of structures than can be be described as eutactic oxygen arrays with one–half of the octahedral interstices occupied by silicon. The availability for considerable polymorphism in the crystalline state provides a viewpoint to describe the high–pressure amorphous state as ordered eutactic arrays of oxygen with the silicon disordered over one–half of the octahedral sites. The sequence of stable phases with increasing pressure is therefore stishovite $\Rightarrow$ $CaCl_2$–type $\Rightarrow$ α–PbO_2–type $\Rightarrow$ $Pa3$–type with the the possibility for considerable metastable crystalline phases at high pressure. Finally, using the shear modulus as a predictor of hardness, we have shown that the post–stishovite phases of silica are not likely to be superhard, let alone harder than diamond.

Chapter 5

Conclusions

5.1 Conclusions

The recent search for superhard materials has concentrated on materials with high bulk moduli due to the assumption that hardness generally scales with the bulk modulus. However, the aggregate shear modulus of a material is a actually a better predictor of hardness. As the predicted shear moduli of a number of C_3N_4 phases are only 60–80% that of diamond, it would appear that the hardness of carbon nitrides should not exceed that of cubic–BN, let alone diamond. While it appears most difficult to design a single phase material with a shear modulus exceeding that of diamond, alloys between diamond–C and cubic–BN should have shear moduli approaching that of diamond and exhibit a number of valuable properties.

Harrison presents an elegant model to explain the high rigidity of diamond.[70] He argues that the carbon tetrahedra in diamond behave as rigid sp^3 hybrids. This bonding state prefers the ideal tetrahedral angles of the diamond structure. The sp^3 carbon tetrahedra are quite resistant to deformation because carbon lacks easy access to the higher electronic states

(such as *d*–states) needed for the rehybidization that would allow these bonds to become more compliant. This explains the high values of the $(C_{11}\text{-}C_{12})/2$ and C_{44} elastic constants that cause the shear modulus of diamond to be so large. It therefore seems quite unlikely to find a single–phase crystalline material with a shear modulus higher than diamond. With the shear modulus shown to be a robust predictor of hardness, this suggests that diamond will remain the hardest known bulk material.

Does this mean that it is impossible to make a material harder than diamond? Not neccessarily; it has been reported that the hardness of thin films can be significantly improved by the creation of superlattices.[22, 75, 181] Significant hardness enhancement has been found for superlattice coatings composed of alternating layers of TiN and VN that result in a hardness superior to that of either of the individual components.[75] It is possible that this type of superlattice hardening is a practical route towards the synthesis of films with hardness rivaling or exceeding that of diamond.

Chapter 6

Future Work

Suggested future directions for the work discussed in this dissertation include extending the methodologies of Zhogolev *et al.* to search through the possible stochiometries in the B-C-N-O system and determine those that are most promising for finding new superhard materials. The database of hardness values and elastic properties in Appendix 2 should be expanded for other materials, given search capablities and be put into the public domain.

Further computational and experimental studies on understanding the nature of the order–disorder phase in high–pressure SiO_2 are suggested. It is likely that this phase is thermodynamically stable under the pressures and temperatures in Earth's lower mantle.

Chapter 7

Bibliography

Bibliography

[1] Ahrens, T. J. (1996), "Geophysical and Material Science Implications of the Post-Stishovite Phase", in Proceedings of Advanced Materials '96, edited by M. Akaishi *et al.*, pp. 1-4, (National Institute for Research in Inorganic Materials, Tsukuba, Japan)

[2] Alam, M., T. DebRoy, R. Roy and E. Breval (1988), "High–Pressure Phases of SiO_2 Made in Air by Fedoseev–Derjarguin Laser Process", *Appl. Phys. Lett.*, **53**, 1687–1689.

[3] Badding, J.V. and D.C. Nesting (1996), "Thermodynamic Analysis of the Formation of Carbon Nitrides Under Pressure", *Chem. Mater.*, **8**, 535–540.

[4] Badding, J.V. (1997), "Solid-State Carbon Nitrides" *Adv. Mater.*, **9**, 877.

[5] Badro, J., D.M. Teter, R.T. Downs, P. Gillet, R.J. Hemley and J.L. Barrat (1997), "Theoretical Study of a Five-Coordinated Silica Polymorph" *Phys. Rev. B*, **56**, 5797–5806.

[6] Badzian, A.R. (1981), "Cubic Boron Nitride–Diamond Mixed Crystals", *Mat. Res. Bull.*, **16**, 1385–1393.

[7] A. Badzian (1984), *Syntezy Wysokocisnieniowe Krysztalow O Strukturze Type Diamentu I Ich Structura Atomowa W Swietle Badan Rentgenowskich*, (ITME, Warsaw).

[8] Badzian, A. (1988), "Superhard Material Comparable in Hardness to Diamond", *Appl. Phys. Lett.*, **53**, 2495–2497.

[9] Bando, Y., S. Nakano and K. Kurashima (1996), "A New Cubic B–C–N Compund Revealed by High–Resolution Analytical Electron Microscopy", *J. Elect. Micro.*, **45**, 135–142.

[10] Belonoshko A.B., L.S. Dubrovinsky and N.A. Dubrovinsky (1996), "A New High-Pressure Silica Phase Obtained by Molecular Dynamics" *Am. Mineral.*, **81**, 785–788.

[11] Birch, F. (1978), "Finite Strain Isotherm and Velocities for Single-Crystal and Polycrystalline NaCl at High Pressures and 300°K", *J. Geophys. Res.*, **83**, 1257-1268.

[12] Boisen, M.B., G.V. Gibbs and M.S.T. Bukowinski (1994), "Framework Silica Structures Generated Using Simulated Annealing with a Potential Energy Function Based on an $H_6Si_2O_7$ Molecule" *Phys. Chem. Min.* **21**, 269–284.

[13] Brookes, C.A. (1981), "Scratch and Indentation Hardness of Crystals", *Phil. Mag. A*, **43**, 529–543.

[14] Bukowinski, M.S.T. and G.H. Wolf (1986), "Equation of State and Stability of Fluorite–Structured SiO_2", *J. Geophys. Res.*, **91**, 4704–4710.

[15] Bundy, F.P. (1974), "Superhard Materials", *Sci. Am.*, **231**, 62–70.

[16] Cahn, R.W. (1996), "Harder Than Diamond?", *Nature*, **380**, 104–105.

[17] Carlsson, A.E., N.W. Ashcroft and A.R. Williams (1984), "Properties of SiO_2 in a High–Pressure Fluorite Structure Phase", *Geophys. Res. Lett.*, **11**, 617–619.

[18] Catlow, C.R.A. and G.D. Price (1990), "Computer Modelling of Solid-State Inorganic Materials", *Nature*, **347**, 243–248.

[19] Ceder, G. (1998), "Computational Materials Science - Predicting Properties from Scratch", *Science*, **280**, 1099–1100.

[20] Ceperley, D.M. and B.J. Alder (1980), "Ground State of the Electron Gas by a Stochastic Method", *Phys. Rev. Lett.*, **45**, 566–568.

[21] Chen, Y., L. Guo and E.G. Wang (1997), "Experimental Evidence for α–and β–Phases of Pure and Crystalline C_3N_4 in Films Deposited on Nickel Substrates", *Phil. Mag. Lett.*, **75**, 155–162.

[22] Chu, X. and S.A. Barnett (1995), "Model of Superlattice Yield Stress and Hardness Enhancements", *J. Appl. Phys*, **77**, 4403–4411.

[23] Cohen, M.L. (1985), "Calculation of Bulk Moduli of Diamond and Zincblende Solids" *Phys. Rev. B*, **32**, 7988–7997.

[24] Cohen, M.L. (1986), "Predicting New Solids and Superconductors" *Science*, **234**, 549–553.

[25] Cohen, M.L. (1989), "Novel Materials from Theory" *Nature*, **338**, 291.

[26] Cohen, M.L. (1991a), "Atomic Theory of Hard Crystals," *J. Hard Mat.*, **2**, 13–27.

[27] Cohen, M.L. (1991b), "Predicting New Solids and their Properties", *Phil. Trans. Soc. Lond. A*, **334**, 501–513.

[28] Cohen, M.L. (1993), "Predicting Useful Materials" *Science*, **261**, 307–308.

[29] Cohen, M.L. (1996), "Structural, Electronic and Optical Properties of Carbon Nitride", *Mat. Sci. Eng. A*, **209**, 1–4.

[30] Cohen, R.E. (1991c), "Bonding and Elasticity of Stishovite SiO_2 at High Pressure: Linearized Augmented Plane Wave Calculations", *Am. Mineral*, **76**, 733–742.

[31] Cohen, R.E. (1992), "First–Principles Predictions of Elasticity and Phase Transitions in High Pressure SiO_2 and Geophysical Implications", in *High–Pressure Research: Applucations to Earth and Planetary Sciences*, edited by Y. Syono and M.H. Manghnani, 425–431 (Terra, Tokyo).

[32] Corkill, J.L. and M.L. Cohen (1993), "Calculated Quasi–Particle Band–Gap of β–C_3N_4", *Phys. Rev. B*, **48**, 17622–17624.

[33] Cote, M. and M.L. Cohen (1997), "Carbon Nitride Compounds With 1:1 Stoichiometry", *Phys. Rev. B*, **55**, 5684-5688.

[34] Cotton, F.A. and G. Wilkinson (1972), *Advanced Inorganic Chemistry*, (Wiley, New York).

[35] Deem, M.W. and J.M. Newsam (1992), "Framework Crystal Structure Solution by Simulated Annealing - Test Application to known Zeolite Structures", *J. Am. Chem. Soc.*, **114**,7189–7198.

[36] DeVries, R.C. (1981), *Synthesis and Properties of Diamond and Cubic Boron Nitride*, Report No. 81CRD110, (General Electric, Schenectady).

[37] DeVries, R.C. (1991), "A Review of Cubic BN and Related Materials", in *Diamond and Diamond–like Films and Coatings*, edited by R.E. Clausing *et al.*, NATO ASI Series B: Vol. 266 (Plenum, New York), 151–172.

[38] Devries, R.C. (1995), "C_3N_4 or Bust", *Diamond and Rel. Mater.*, **4**, 1093–1094.

[39] Duan, Y., K. Zhang and X. Xie (1997), "Electronic Structural Properties of β–C_3N_4, β–Si_3N_4 and β–Ge_3N_4", *Phys. Stat. Sol. B*, **200**, 499–508.

[40] Dubrovinsky, L.S., S. K. Saxena, P. Lazor, R. Ahuja, O. Eriksson, J.M. Wills and B. Johansson (1996), "Experimental and Theoretical Identification of a New High-Pressure Phase of Silica", *Nature*, **388**, 362–365.

[41] Endo T., T. Sato, and M. Shimada (1987), "High Pressure Synthesis of B_2O with Diamond–like Structure", *J. Mat. Sci. Lett.*, **11**, 683–685.

[42] Fang, P.H. (1995), "On the β–C_3N_4 Search", *J. Mater. Sci. Lett.*, **14**, 536–538.

[43] Gerk, A.P. (1977), "The Effect of Work-Hardening Upon the Hardness of Solids: Minimum Hardness" *J. Mat. Sci*, **12**, 735–738.

[44] Gerlich, D., S. Hart and D. Whittal (1984), "Pressure Derivatives of the Elastic Moduli of the Rutile–Structure Difluorides", *Phys. Rev. B*, **29**, 2142–2147.

[45] German, V.N., M.A. Podurets and R.F. Trunin (1973), "Synthesis of a High–Density Phase of Silicon Dioxide in Shock Wave", *Sov. Phys. JETP* **37**, 107.

[46] Gibbs, G.V., M.B. Boisen, R.T. Downs and A.C. Lasaga (1988), "Mathematical Modeling of the Structures and Bulk Moduli of TX_2 quartz and Cristobalite Structure–Types, T= C, Si, Ge and X = O, S", *Mat. Res. Soc. Symp. Proc.*, **121**, 155–165.

[47] Gilman, J.J. (1968) "Escape of Dislocations from Bound States by Tunneling" *J. Appl. Phys.*, **39**, 6086–6090.

[48] Gilman, J.J. (1973), "Hardness of Pure Alkali Halides", *J. Appl. Phys.*, **44**, 982–984.

[49] Gilman, J.J. (1993), "Why Silicon is Hard", *Science*, **261**, 1436–1439.

[50] Gilman, J.J. (1995), "The Unique Strength of Diamond", in *Mechanical Behavior of Diamond and Other Forms of Carbon*, edited by M.D. Drory, D.B. Bogy, M.S. Donley, and J.E. Field, (Materials Research Society, Pittsburgh) p. 281.

[51] Gilman, J.J. (1996), "Physical Chemistry of Intrinsic Hardness", *Mat. Sci. Eng. A*, **209**, 74–81.

[52] Gilman, J.J. (1997), "Chemical and Physical "Hardness"", *Mat. Res. Innov.*, **1**, 72–76.

[53] Goble, R.J. and S.D. Scott (1985), "The Relationship between Mineral hardness and Compressibility (or Bulk Modulus)" *Can. Min.*, **23**, 273–285.

[54] Grimsditch, M. and A.K. Ramdas (1975), "Brillouin Scattering in Diamond", *Phys. Rev. B*, **11**, 3139–3148.

[55] Grimsditch, M., E.S. Zouboulis and A. Polian (1994), "Elastic Constants of Boron Nitride", *J. Appl. Phys.*, **76**, 832–834.

[56] Grimsditch, M. (1984), "Polymorphism in Amorphous SiO_2" *Phys. Rev. Lett.*, **52**, 2379–2381.

[57] Grimvall,G and M. Thiessen (1986), in *Science of Hard Materials*, Proc. of the Int. Conf. Science of Hard Materials 1984, Institute of Physics Conference Series Number 75, p. 61, (Adam Hilger Ltd, Boston).

[58] Grumbach, M.P., O.F. Sankey, and P.F. McMillan (1995), "Properties of B_2O: An Unsymmetrical Analog of Carbon", *Phys. Rev. B*, **52**, 15807–15811.

[59] Guo, L.P, Y. Chen, E.G. Wang, L. Li and Z.X. Zhao (1997), "Identification of a New C–N Phase with Monoclinic Structure", *Chem. Phys. Lett.*, **268**, 26–30.

[60] Y. Guo and W.A. Goddard (1995), "Is Carbon Nitride Harder than Diamond? - No, But Its Girth Increases When Stretched (Negative Poisson Ratio)", *Chem. Phys. Lett.*, **237**, 72–76.

[61] Haines, J. and J.M. Léger (1993), "Phase Transitions in Ruthenium Dioxide up to 40 GPa: Mechanism for the Rutile to Fluorite Phase Transformation and a Model for the High Pressure Behavior of Stishovite SiO_2", *Phys. Rev. B*, **48**, 13344–13350.

[62] Haines, J., J.M. Léger and O. Schulte (1996a), "The High–Pressure Phase Transition Sequence from the Rutile–Type through to the Cotunnite–Type Structure in PbO_2", *J. Phys. Condens. Matter*, **8**, 1631–1646.

[63] Haines, J., J.M. L/'eger and O. Schulte (1996b), "$Pa\overline{3}$ Modified Fluourite–Type Structures in Metal Dioxides at High Pressure", *Science*, **271**, 629–631.

[64] Haines, J. and J.M. Léger (1997), "X–Ray Diffraction Study of the Phase Transitions and Structural Evolution of Tin Dioxide at High Pressure: Relationships Between Structure Types and Implication for Other Rutile–Type Dioxides", *Phys. Rev. B*, **55**, 11144–11154.

[65] Haines J., J.M. Léger, M.W. Schmidt, J.P. Petitet, A.S. Pereira, J.A.H. Da Jornada and S. Hull (1998), "Structural Characterisation of the $Pa\overline{3}$–type High Pressure Phase of Ruthenium Dioxide", *J. Phys. Chem. Solids*, **59**, 239–243.

[66] Hall, T.H. (1965), *Science*, **148**, 1331–.

[67] Hall, T.H. and L.A. Compton (1965), "Group IV Analogs and High Pressure, High temperature Synthesis of B_2O", *Inorg. Chem.*, **4**, 1213–1216.

[68] Han, H.X. and B.J. Feldman (1988), "Structural and Optical Properties of Amorphous Carbon Nitride", *Solid State Comm.*, **65**, 921–923.

[69] Han, S. and J. Ihm (1997), "Structural and Electronic Properties of Diamond With Hypothetical Vacancies Stabilized by Nitrogen or Boron Atoms", *Phys. Rev. B*, **55**, 15349–15352.

[70] Harrison, W.A. (1980), in *Electronic Structure and the Properties of Solids*, (W.H. Freeman, San Fancisco) p. 185.

[71] Hashin, Z. and S. Shtrikman (1962), *J. Mech. Phys. Solids*, **10**, 335–343.

[72] Hazen, R.M. and L.W. Finger (1981), "Bulk Moduli and High Pressure Crystal Structures of Rutile–Type Compounds", *J. Phys. Chem. Solids*, **42**, 143–151.

[73] Hazen, R.M. and L.W. Finger (1982), *Comparative Crystallography* (John Wiley, Chichester).

[74] Hazen, R.M., L.W. Finger, R.J. Hemley and H.K. Mao (1989), "High–Pressure Crystal Chemistry and Amorphization of α–Quartz", *Solid State Comm.*, **72**, 507–511.

[75] Helmersson, U., S. Todorova, S.A. Barnett, J.E. Sundgren, L.C. Markert and J.E. Greene (1987), "Growth of Single-Crystal TiN/VN Strained-Layer Superlattices with Extremely High Mechanical Hardness" *J. Appl. Phys.*, **62**, 481–484.

[76] Hemley, R.J., C.T. Prewitt, and K.J. Kingma (1994), *Silica: Physical Behavior, Geochemistry, and Materials Applications*, Reviews in Mineralogy, Vol. 29, (MSA, Washington, DC).

[77] Hohenberg, P and W. Kohn (1964), *Phys. Rev.*, **136**, B864–.

[78] Hughbanks, T. and Y. Tian (1995), "On the Structure and Composition of Carbon Nitride", *Sol. State Commun.*, **96**, 321–325.

[79] Hyde, B.G., L.A. Bursill, M. O'Keeffe and S. Andersson (1972), "Continuous Topological Variation of Coordination in Crystals: Structural Relations and Possible Transformation Mechanisms", *Nature*, **237**, 35–38.

[80] Hyde, B.G. and S. Andersson (1989), *Inorganic Crystal Structures*, (Wiley, New York).

[81] Ivan'ko, A.A. (1971), *Handbook of Hardness Data* (translated from Russian), (Keter, Jerusalem).

[82] Jin, W., R.K. Kalia, P. Vashishta and J.P. Rino (1993), "Structural Transformation, Intermediate–Range Order, and Dynamical Behavior of SiO_2 Glass at High Pressures", *Phys. Rev. Lett.*, **71**, 3146–3149.

[83] Jin, W., R.K. Kalia, P. Vashishta and J.P. Rino (1994), "Structural Transformation in Densified Silica Glass: A Molecular–Dynamics Study", *Phys. Rev. B*, **50**, 118–131.

[84] Jolly, L.H., B. Silvi and P. d'Arco (1993), "Periodic Hartree–Fock Investigation of the Stishovite $CaCl_2$–like Phase Transition of Silica", *J. Chim. Phys.*, **90**, 1887–1895.

[85] Julg, A. (1987), "An Empirical Relationship between Hardness and Bond Ionicity in Crystals", *Phys. Chem. Min.*, **3**, 45–53.

[86] Julian, M.M. and G.V. Gibbs (1988), "Modeling the Configuration about the Nitrogen Atom in Methyl– and Silyl–Substituted Amines", *J. Phys. Chem.*, **92**, 1444–1451.

[87] Kakudate, Y.,M. Yoshida, S. Usuba, H. Yokoi, S. Fujiwara, M. Kawaguchi, K. Sako and T. Sawai (1993), *Proc. 3rd IUMRS Int. Conf. Adv. Mater., Tokyo.*

[88] Kanzaki, M., Y. Matsui and M. Matsui (1997), "A New High–Pressure Silica Phase Obtained by Molecular Dynamics–Discussion", *Am. Mineral.*, **82**, 1042.

[89] Karki, B.B., M.C. Warren, L. Stixrude, G.J. Ackland and J. Crain (1997a), "Ab Initio Studies of High–Pressure Structural Transformations in Silica", *Phys. Rev. B*, **55**, 3465–3471.

[90] Karki, B.B., M.C. Warren, L. Stixrude, G.J. Ackland and J. Crain (1997b), "Erratum: Ab Initio Studies of High–Pressure Structural Transformations in Silica", *Phys. Rev. B*, **56**, 2884.

[91] Karki, B.B., L. Stixrude and J. Crain (1997), "Ab Initio Elasticity of Three High–Pressure Polymorphs", *Geophys. Res. Lett.*, **24**, 3269-3272.

[92] Kawaguchi, M. (1997), "B/C/N Materials Based on the Graphite network", *Adv. Mater.*, **9**, 615–625.

[93] Keskar, N.R., J.R. Chelikowsky and R.M. Wentzcovitch (1994), "Mechanical Instabilities in $AlPO_4$", *Phys. Rev. B*, **50**, 9072–9078.

[94] Kingma, K.J., R.E. Cohen, R.J. Hemley and H.K. Mao (1995), "Transformation of Stishovite to a Dense Phase at Lower–Mantle Pressures", *Nature*, **374**, 243–245.

[95] Kingma, K.J., H.K. Mao, and R.J. Hemley (1996), "Synchrotron X–Ray Diffraction of SiO_2 to Multimegabar Pressures", *High Pressure Res.*, **14**, 363–374.

[96] Kisly, P.S. (1986), in *Science of Hard Materials*, Proc. of the Int. Conf. Science of Hard Materials 1984, Institute of Physics Conference Series Number 75, p. 107, (Adam Hilger Ltd, Boston).

[97] Kohn, W. and L.J. Sham (1965), *Phys. Rev.*, **140**, A1133–.

[98] Komatsu, T., M. Nomura, Y. Kakudate and S. Fujiwara (1996), "Synthesis and Characterization of a Shock-Synthesized Cubic B-C-N Solid Solution of Composition $BC_{2.5}N$", *J. Mater. Chem.*, **6**, 1799–1803.

[99] Komatsu, T., Y. Kakudate and S. Fujiwara (1996), "Heat Resistance of a Shock-Synthesized B-C-N Heterodiamond", *J. Chem. Soc., Faraday Trans.* **92**, 5067–5071.

[100] Komatsu, T. (1998), "Thermal Expansion Behavior of a Shock-Synthesized B-C-N Heterodiamond", *J. Chem. Soc. Faraday Trans.*, **94**, 101–104.

[101] Knittle, E., R.B. Kaner, R. Jeanloz and M.L. Cohen (1995), "High–Pressure Synthesis, Characterization, and Equation of State of Cubic C–BN Solid Solutions", *Phys. Rev. B*, **51**, 12149–12155.

[102] Kouvetakis, J., A. Bandari, M. Todd, B. Wilkens and N Cave (1994), "Novel Synthetic Routes to Carbon–Nitrogen Thin Films", *Chem. Mater.*, **6**, 811–814.

[103] Kusaba, K., M. Kikuchi, K. Fukuoka and Y. Syono (1988), "Anisotropic Phase Transition of Rutile under Shock Compression", *Phys. Chem. Mineral.*, **15**, 238–245.

[104] Lacks, D.J. and R.G. Gordon (1993), "Calculations of Pressure–Induced Phase Transitions in Silica", *J. Geophys. Res.*, **98**, 22147–22155.

[105] Lambrecht, W.R.L. and B. Segall (1993), "Anamalous Band–Gap Behavior and Phase Stability of c-BN–Diamond Alloys", *Phys. Rev. B*, **47**, 9289–9296.

[106] Lee, C. and X. Gonze (1994), "Lattice Dynamics and Dielectric Properties of SiO_2 Stishovite", *Phys. Rev. Lett.*, **72**, 1686–1689.

[107] Lee, C. and X. Gonze (1995), "The Pressure–Induced Ferroelastic Phase Transition of SiO_2 Stishovite", *J. Phys. Condens. Matter*, **7**, 3693–3698.

[108] Lee, C. (1996), "Analyses of the Ab Initio Harmonic Interatomic Force Constants of Stishovite", *Phys. Rev. B*, **54**, 8973–8976.

[109] Léger, J.M., J. Haines and B. Blanzat (1994), "Materials Potentially Harder than Diamond: Quenchable High–Pressure Phases of Transition Metal Dioxides", *J. Mat. Sci. Lett.*, **13**, 1688–1690.

[110] Léger, J.M., J. Haines, M. Schmidt, J.P. Petitet, A.S. Pereira and J.A.H. da Jornada (1996), "Discovery of Hardest Known Oxide", *Nature*, **383**, 401.

[111] Léger, J.M. and J. Haines (1997), "The Search for Superhard Materials", *Endeavour*, **21**, 121–124.

[112] Li, D., E. Cutiongco, Y.W. Chung, M.S. Wong and W.D. Sproul (1995), "Review of Synthesis and Characterization of Amorphous–Carbon Nitride Thin–Films", *Diamond Films and Tech.*, **5**, 261–273.

[113] Lieber, C.M. and Z.J. Zhang (1994), "Synthesis of Covalent Carbon–Nitride Solids - Alternatives to Diamond", *Adv. Mater.*, **6**, 497-499.

[114] Lieber, C.M. and Z.J. Zhang, "Carbon–Nitride Solids - Potential Alternatives to Diamond", *Chem. and Ind.*, **22**,922–925.

[115] Lima de Faria, J. (1994), *Structural Mineralogy: An Introduction*, (Kluwer, Boston).

[116] Liu, A.Y. and M.L. Cohen (1989), "Prediction of New Low–Compressibility Solids", *Science*, **245**, 841–842.

[117] Liu, A.Y., R.M. Wentzcovitch and M.L. Cohen (1989), "Atomic Arrangement and Electronic Structure of BC_2N", *Phys. Rev. B*, **39**, 1760–1765.

[118] Liu, A.Y. and M.L. Cohen (1990), "Structural Properties and Electronic Structure of Low–Compressibility Materials: β–Si_3N_4 and Hypothetical β–C_3N_4", *Phys. Rev. B*, **41**, 10727–10734.

[119] Liu, A.Y. and R.M. Wentzcovitch (1994), "Stability of Carbon Nitride Solids", *Phys. Rev. B*, **50**, 10362–10365.

[120] Liu, A.Y. (1996), in *Quantum Theory of Real Materials*, edited by J. R. Chelikowsky and S. G. Louie, (Kluwer, Boston).

[121] Liu, L.G., W.A. Bassett and T. Takahashi (1974a), "Effect of Pressure on the Lattice Parameters of Stishovite", *J. Geophys. Res.*, **79**, 1160–1164.

[122] Liu, L.G. (1974b), "Synthesis of a New High–Pressure Phase of Tin Dioxide and some Geophysical Implications", *Phys. Earth Plan. Int.*, **9**, 338–343.

[123] Liu, L.G. (1978), "A Fluorite Isotype of SnO_2 and a New Modification of TiO_2: Implications for the Earth's Lower Mantle", *Science*, **199**, 422–425.

[124] Liu, L.G., W.A. Bassett and J. Sharry (1978), "New High–Pressure Modifications of GeO_2 and SiO_2", *J. Geophys. Res.*, **83**, 2301–2305.

[125] Liu, X.Y., X.D. Zhao and W.H. Su (1994), "High Pressure Synthesis of Serial Higher Boron Suboxides With Cage Structures", in *High Pressure Science and Technology: AIRAPT-1993* (AIP, 1994), p. 1279–1282.

[126] Lundin, U., L. Fast, L. Nordstrom, J.M. Wills, B. Johansson and O. Eriksson (1998), "Transition-Metal Dioxides with a Bulk Modulus Comparable to Diamond" *Phys. Rev. B*, **57**, 4979–4982.

[127] Martin-Gil, J., F.J. Martin-Gil, M. Sarikaya, M. Qian, M. José–Yacamán and A. Rubio (1997), "Evidence of a Low Compressibility Carbon Nitride with Defect–Zincblende Structure", *J. Appl. Phys.*, **81**, 2555–2559.

[128] Marton, D., K.J. Boyd, and J.W. Rabalais (1995), "Synthesis of Carbon Nitride", *Int. J. Mod. Phys.*, **9**, 3527–3558.

[129] Marumo, F. and Y. Syono (1971), "The Crystal Structure of Zn_2SiO_4-II: A high–pressure phase of Willemite", *Acta. Cryst. B*, **27**, 1868–.

[130] Matsui, Y. and K. Kawamura (1987), "Computer–Experimental Synthesis of Silica with the α–PbO_2 Structure", *High–Pressure research in Mineral Physics* (eds. M.H. Manghnani and Y. Syono), 305–311, (Terra, Tokyo).

[131] Matsui, Y. and M. Matsui (1988), "Molecular Dynamics Studies of Polymorphism of SiO_2 at High Pressures: A Possible New Cubic Polymorph with High Density", *Advances in Physical Geochemistry* Vol. 7 (eds. S. Ghose, E. Salje, and J.M.D. Coey) 129–140, (Springer, New York).

[132] McColm, I.J. (1990), *Ceramic Hardness*, (Plenum, New York).

[133] McNeil, L.E. and M. Grimsditch (1992), "Pressure–Amorphized SiO_2 α–Quartz: An anisotropic Amorphous Solid.", *Phys. Rev. Lett.*, **68**, 83–85.

[134] McQueen, R.G., J.C. Jamieson and S.P. Marsh (1967), "Shock–Wave Compression and X–Ray Studies of Titanium Dioxide", *Science*, **155**, 1401–1404.

[135] Meade, C., R.J. Hemley and H.K. Mao (1992), "High–Pressure X–Ray Diffraction of SiO_2 Glass", *Phys. Rev. Lett.*, **69**, 1387-1390.

[136] Mehl, M.J., B. M. Klein, and D. A. Papaconstantopoulos (1994), "First–Principles Calculation of Elastic Properties", in *Intermetallic Compounds, Principles and Practice*, Vol. I, edited by J. H. Westbrook and R. L. Fleischer (John Wiley and Sons, London), Ch. 9.

[137] Ming, L.C. and M.H. Manghnani (1983), "High–Pressure Phase Transformations in Vitreous and Crystalline GeO_2 (Rutile)", *Phys. Earth. Planet. Int.*, **33**, 26–30.

[138] Mitas, L. and R.M. Martin (1994), "Quantum Monte–Carlo of Nitrogen- Atom, Dimer, Atomic, and Molecular Solids", *Phys. Rev. Lett.*, **72**, 2438–2441.

[139] Mitas, L. (1996), "Electronic Structure by Quantum Monte Carlo: Atoms, Molecules and Solids", *Comp. Phys. Comm.*, **96**, 107–117.

[140] Montigaud, H., B. Tanguy, G. Demazeau, S. Courjault, M. Birot and J. Dunogues (1997), "Sur la Synthese de C_3N_4 de structure Graphitique par Voie Solvothermale", *C.R. Acad. Sci. Paris*, **325**, 229–234.

[141] Morita, N., T. Endo, T. Sato and M. Shimada (1987), "TiF_2 With Fluorite Structure – A New Compound", *???*, **??**, 859–861.

[142] Müller, V.E. (1982), "Zur Struktur von $CaPdF_4$, $CdPdF_4$, $HgPdF_4$ und HP-PdF_2", *J. Fluor. Chem.*, **20**, 291-299.

[143] Müller, V.E. (1984), *Acta. Cryst. B*, **40**, 359–.

[144] Nagel, L. and M. O'Keeffe (1971), "Pressure and Stress Induced Polymorphism of Compounds with Rutile Structure" *Mat. Res. Bull.* **6**, 1317–1320.

[145] Nakano, S., M. Akaishi, T. Sasaki, and S. Yamaoka (1994), "Segregative Crystallization of Several Diamond–like Phases from the Graphitic BC_2N Without an Additive at 7.7 GPa", *Chem. Mater.*, **6**, 2246–2251.

[146] Nakano, S., M. Akaishi, T. Sasaki and S. Yamaoka (1996), "Characterization of Several Cubic Phases Directly Transformed From the graphitic BC_2N", *Mat. Sci. Eng. A*, **209**, 26–29.

[147] Nesting, D.C. and J.V. Badding (1996), "High-Pressure Synthesis of sp^2-bonded Carbon Nitrides", *Chem. Mater.*, **8**, 1535-1539.

[148] Nguyen, J.H. and R. Jeanloz (1996), "Initial Description of a New Carbon–Nitride Phase Synthesized at High Pressures and Temperatures", *Mat. Sci. Eng. A*, **209**, 23–25.

[149] Niemyski, T., S. Appenheimer, J. Panczyk, and A. Badzian (1969), *J. Cryst. Growth*, **5**, 401–.

[150] Nishidata, K., M. Baba, T. Sato and K. Nishikawa (1995), "Molecular Dynamics Studies on the Shock–Induced Phase Transition of a MgF_2 Crystal", *Phys. Rev. B*, **52**, 3170–3176.

[151] O'Keeffe, M. (1977), "On the Arrangement of Ions in Crystals", *Acta Cryst. A*, **33**, 924–927.

[152] Omaly, P.J., P. Batail, D. Grandjean, D. Avignant and J.C. Cousseins (1976), "The Crystal Structure of α–$NaTiF_4$" *Acta. Cryst. B*, **32**, 2106–2110.

[153] O'Neill, H (1934), *The Hardness of Metals and Its Measurement*, (Chapman and Hall, London).

[154] Ortega, J. and O.F. Sankey (1995), "Relative Stability of Hexagonal and Planar Structures of Hypothetical C_3N_4 Solids", *Phys. Rev. B*, **51**, 2624–2627.

[155] Park, K.T., K. Terakura and Y. Matsui (1988), "Theoretical Evidence for a New Ultrahigh–Pressure Phase of SiO_2", *Nature*, **336**, 670–672.

[156] Parthé, E. (1964), "Crystal Chemistry of Tetrahedral Structures", (Gordon and Breach, New York).

[157] Pauling, L. and J.H. Sturdivant (1928), "The Crystal Structure of Brookite", *J. Am. Chem. Soc.*, **XX**, 239–256.

[158] Payne, M.C., M.P. Teter, D.C. Allan, T.A. Arias and J.D. Joannopoulos (1992), "Iterative Minimization Techniques for Abinito Total–Energy Calculations - Molecular–Dynamics and Conjugate Gradients", *Rev. Mod. Phys.*, **64**, 1045–1097.

[159] Peacock, M.A. and A.S. Dadson (1940), "On Rammelsbergite and Pararammelsbergite: Distinct Forms of Nickel Diarsenide", *Am. Mineral.*, **25**, 561–577.

[160] Perdew, J.P., J.A. Chevary, S.H. Vosko, K.A. Jackson, M.R. Pederson, D.J. Singh and C. Fiolhais (1992), "Atoms, Molecules, Solids, and Surfaces: Applications of the Generalized Gradient Approximation for Exchange and Correlation", *Phys. Rev. B*, **46**, 6671-6687.

[161] Pettifor, D.G. (1996), "Phenomenology and Theory in Structural Prediction", *J. Phase Equil.*, **17**, 384–395.

[162] Plendl, J.N. and P.J. Gielisse (1961), "Hardness of Nonmetallic Solids on an Atomic Basis", *Phys. Rev*, **125**, 828–832.

[163] Plendl, J.N., S.S. Mittra and P.J. Gielisse (1965), *Phys. Stat. Solidi*, **12**, 367–.

[164] Podurets, M.A., G.V. Simakov and R.F. Trunin (1990), "Stishovite Transition to a Denser Phase", *Izv. Phys. Solid Earth*, **26**, 295–300.

[165] Primak, W. (1975), *The Compacted States of Vitreous Silica*, see pg. 81. (Gordon and Breach, New York).

[166] Reyes–Serrato, A., D.H. Galván and I.L. Garzön (1995), "Ab Initio Hartree–Fock Study of Structural and Electronic Properties of β–Si_3N_4 and β–C_3N_4 Compounds", *Phys. Rev. B*, **52**, 6293–6300.

[167] Riedel, R. (1992), "Materials Harder Than Diamond", *Adv. Materials*, **4**, 759–761.

[168] Riedel, R. (1994), "Novel Ultrahard Materials", *Adv. Materials*, **6**, 549–560.

[169] Robertson, J. (1981), *Philos. Mag. B*, **44**, 215–.

[170] Rosenblum, S.S., W.H. Weber and B.L Chamberland (1997), "Raman–Scattering Observation of the Rutile to $CaCl_2$ Phase Transition in RuO_2", *Phys. Rev. B*, **56**, 529–533.

[171] Ross, N.L., J.F. Shu, R.M. Hazen and T. Gasparik (1990), "High–Pressure Crystal Chemistry of Stishovite", *Amer. Mineral.*, **75**, 739–747.

[172] Sasaki, T., M. Akaishi, S. Yamaoka, Y. Fujiki and T. Oikawa (1993), "Simultaneous Crystallization of Diamond and Cubic Boron Nitride from the Graphite Relative BC_2N under High Pressure/High Temperature Conditions", *Chem. Mater.*, **5**, 695–699.

[173] Schnick, W. (1993), "Carbon (IV) Nitride C_3N_4 - A New material Harder than Diamond", *Agnew. Int. Ed. Engl.*, **32**, 1580–1581.

[174] Sekine, T., M. Akaishi and N. Setaka (1987), "Fe_2N–Type SiO_2 From Shocked Quartz", *Geochim. Cosmochim. Acta*, **51**, 379–381.

[175] Sekine, T., H. Kanda, Y. Bando, M. Yokoyama and K. Hojou (1990), "A Graphitic Carbon Nitride", *J. Mat. Sci. Lett.*, **9**, 1376–1378.

[176] Simakov, G.V., M.A. Podurets and R.F. Trunin (1973), "New Data on the Compressibility of Oxides and Fluorides and the Theory of Homogeneous Composition of the Earth", *Doklady Akad. Nauk SSSR*, **211**, 29–31.

[177] Sirota, N.N. and M.M. Zhuk (1979), *Vestsi Akad. Navuk BSSR, Ser. Fiz.-Mat. Navuk*, **3**, 122–.

[178] Sjöström, H., S. Stafström, M. Boman and J.E. Sundgren (1995), "Superhard and Elastic Carbon Nitride Thin Films having a Fullerenelike Microstructure", *Phys. Rev. Lett.*, **75**, 1336–1339.

[179] Small, L. (1966), *Hardness: Theory and Practice*, (Ferndale, Michigan).

[180] Spackman, M.A., R.J. Hill and G.V. Gibbs (1987), "Exploration of Structure and Bonding in Stishovite with Fourier and Pseudoatom Refinement Methods Using Single Crystal and Powder X–Ray Diffraction Data", *Phys. Chem. Min.*, **14**, 139–150.

[181] Sproul, W.D. (1996), "New Routes in the Preparation of Mechanically Hard Films", *Science*, **273**, 889–892.

[182] Srikanth, V., R. Roy, E.K. Graham and D.E. Voigt (1991), "B_xO Phases Present at High Pressure and Temperature", *J. Am. Chem. Soc.*, **74**, 3145–3147.

[183] Stevens, A.J., T. Koga, C.B. Agee, M.J. Aziz and C.M. Lieber (1996), "Stability of Carbon Nitride Materials at High Pressure and Temperature", *J. Am. Chem. Soc.*, **118**, 10900–10901.

[184] Stishov, S.M. and S.V. Popova (1961), "A New Dense Modification of Silica", *Geokhimiya*, **10**, 837–.

[185] Sturdivant, J.H. (1930?), "The Crystal Structure of Columbite", *??????????*, **??**, 88–108.

[186] Subrayan, R.P. and P.G. Rasmussen (1995), "An Overview of Materials Composed of Carbon and Nitrogen", *Trends Poly. Sci.*, **3**, 165–172.

[187] Sumya, H. (1989), *High–Hardness, Cubic Boron Nitride Sintered Body and its Preparation*, JP 89-208,371.

[188] Sun, C.Q. (1998), "A Model For Bonding and Band–Forming For Oxides and Nitrides", *Appl. Phys. Lett.*, **72**, 1706–1708.

[189] Sung, C.M. and M. Sung (1996), "Carbon Nitride and Other Speculative Superhard Materials", *Mat. Chem. and Phys.*, **43**, 1–18.

[190] Syono, Y., S. Akimoto and Matsui, Y. (1971), *J. Solid State Chem.*, **3**, 369–.

[191] Szymanski, A. and J.M. Szymanski (1989), *Hardness Estimation of Minerals, Rocks and Ceramic Materials*, Elsevier, Amsterdam).

[192] Tabor, D. (1951), *The Hardness of Metals*, (Clarendon, Oxford).

[193] Tabor, D. (1970), *Rev. of Phys. in Tech.*, **1**, 145–.

[194] Tabor, D. (1986), in *Microindentation Techniques in Materials Science and Engineering*, edited by P.J. Blau and B.R. Lawn ASTM STP 889 (ASTM, Philadelphia) p. 129.

[195] Tabor, D. (1996), "Indentation Hardness: Fifty Years on - A Personal View", *Phil. Mag. A*, **74**, 1207–1212.

[196] Tateyama, Y., T. Ogitsu, K. Kusakabe, S. Tsuneyuki and S. Itoh (1997), "Proposed Synthesis Path for Heterodiamond BC_2N", *Phys. Rev. B*, **55**, 10161–10164.

[197] Teter, D.M. and R.J. Hemley (1996), "Low–Compressibility Carbon Nitrides", *Science*, **271**, 53–55.

[198] D.M. Teter and N.W. Ashcroft, (unpublished manuscript).

[199] Teter, D.M. (1998), "Computational Alchemy: The Search for New Superhard Materials", *MRS Bull.*, **23**, 22–27).

[200] Teter, D.M. (1999), In preparation.

[201] Teter, D.M. and R.J. Hemley (1998), "High Pressure Polymorphism in Silica", *Phys. Rev. Lett.*, **80**, 2145–2148.

[202] Tossell, J.A. (1980), "Theoretical Study of Structures, Stabilities, and Phase Transitions in some Metal Dihalide and Dioxide Polymorphs", *J. Geophys. Res.*, **85**, 6456–6460.

[203] Tossell, J.A. (1997), "Second Nearest–Neighbor Effects upon N NMR Shieldings in Models for Si_3N_4 and C_3N_4", *J. Mag. Res.*, **127**, 49–53.

[204] Tressaud, A., F. Langlais, G. Demazeau and P. Hagenmuller (1979), "Sur Une Variete Haute Pression de PdF_2 de Type Fluoride", *Mat. Res. Bull.*, **14**, 1147–1153.

[205] Tressaud, A. and G. Demazeau (1984), "The High–Pressure Form of PdF_2: An Alternative Model for the High–Pressure Polymorphic Sequence of Rutile Compounds", *High Temp - High Press.*, **16**, 303–308.

[206] Trunin, R.F., G.V. Simakov, M.A. Podurets, B.N. Moiseyev and I.V. Popov (1971), "Dynamic Compressibility of Quartz and Quartzite at High Pressure", *Phys. Solid Earth*, **1**, 8–12.

[207] Trunin, R.F., M.A. Podurets, G.V. Simakov, L.V. Popov and A.G. Sevast'yanov (1995), "New Data, Obtained Under Strong Shock Wave Conditions from an Underground Nuclear Explosion, on the Compressibility of Aluminum, Plexiglass, and Quartz", *Zh. Eksper. i Teoret. Fiziki*, **108**, 851–861.

[208] Tse, J.S. and D.D. Klug (1991a), "The Structure and Dynamics of Silica Polymorphs Using a Two–Body Effective Potential Model", *J. Chem. Phys.*, **95**, 9176–9185.

[209] Tse, J.S. and D.D. Klug (1991b), "Mechanical Instability of α–Quartz: A Molecular Dynamics Study", *Phys. Rev. Lett.*, **67**, 3559–3562.

[210] Tse, J.S., D.D. Klug and Y. Le Page (1992), "Novel High Pressure Phase of Silica", *Phys. Rev. Lett.*, **69**, 3647–3649.

[211] Tse, J.S., D.D. Klug and D.C. Allan (1995), "Structure and Stability of Several High–Pressure Crystalline Polymorphs of Silica", *Phys. Rev. B*, **51**, 16392–16395.

[212] Tse, J.S., D.D. Klug, Y. Le Page and M. Bernasconi (1997), "High–Pressure Four–Coordinated Structure of SiO_2", *Phys. Rev. B*, **56**, 10878–10881.

[213] Tsuchida, Y. and T. Yagi (1989), "A New, Post–Stishovite High–Pressure Polymorph of Silica", *Nature*, **340**, 217–220

[214] Tsuchida, Y. and T. Yagi (1990), "New Pressure-Induced Transformations of Silica at Room Temperature", *Nature*, **347**, 267–269.

[215] Tsuneyuki, S., M. Tsukada, H. Aoki, and Y. Matsui (1988), "First-Principles Interatomic Potential of Silica Applied to Molecular Dynamics" *Phys. Rev. Lett.*, **61**, 869–872.

[216] Tsuneyuki, S., Y. Matsui, H. Aoki and M. Tsukada (1989), "New Pressure–Induced Structural Transformations in Silica Obtained by Computer Simulation", *Nature*, **339**, 209–211.

[217] Urusov, V.S., N.R. Khisina and A.G. Christy (1996), "Quasi–Equilibrium Behaviour of TiO_2–SnO_2 Solid Solutions at High Pressures and Temperatures: The Influence of Non-Hydrostaticity", *Eur. J. Mineral.*, **8**, 791–804.

[218] van Beest, B.W.H. G.J. Kramer, and R.A. van Santen (1990), "Force Fields for Silicas and Aluminophosphates based on Ab Initio Calculations", *Phys. Rev. Lett.*, **64**, 1955-1958.

[219] Vanderbilt, D. (1990), "Soft Self-Consistent Pseudopotentials in a Generalized Eigenvalue Formalism", *Phys. Rev. B*, **41** 7892–7895.

[220] Vrel, D., J.P. Petitet, X. Huang and T. Mashimo (1997), "Synthesis of Ruthenium Oxide High Pressure Phases by Shock Compression" *Physica B* , **239**, 9–12.

[221] Vvedensky, D.D., S. Crampin, M.E. Eberhart and J.M. MacLaren (1990), "Quantum Mechanics and Mechanical Properties: Towards Twenty–First Century Materials", *Cont. Phys.*, **31**, 73–97.

[222] Wang, E.G., Y. Chen and L. Guo (1997), "Synthesis and Characterization of Pure Crystalline C–N Film", *Phys. Scripta*, **T69**, 108–114.

[223] Wedlake, R.J. and A.L. Penny (1978), *Synthesis of a Hard Material*, Ger. Offen. 2,806,070; 8/17/78; filed 2/16/77.

[224] Wells, A.F. (1984), *Structural Inorganic Chemistry* 5th ed., (Clarendon Press, Oxford)

[225] Wentzcovitch, R.M., C. da Silva, J.R. Chelikowsky and N. Binggeli (1998), "A New Phase and Pressure Induced Amorphization in Silica", *Phys. Rev. Lett.*, **80**, 2149–2152.

[226] Yahagi, Y., T. Yagi, H. Yamawaki and K. Aoki (1994), "Infrared Absorption Spectra of the High–Pressure Phases of Cristobalite and their Coordination Numbers of Silicon Atoms", *Solid State. Comm.*, **89**, 945–948.

[227] Yamakata, M. and T. Yagi (1997), "New Stishovite–Like Phase of Silica Formed by Hydrostatic Compression of Cristobalite", *Proc. Japan Acad. B*, **73**, 85–88.

[228] Yamamoto, K., Y. Koga, K. Yase, S. Fujiwara and M. Kubota (1997), "Formation of Cubic Phase Carbon Nitride Solid by Low Energy Nitrogen Implantation into Graphite", *Jpn. J. Appl. Phys.*, **36**, L230–L233.

[229] Yang, W. R.G. Parr, and L. Uytterhoeven (1987), " *Phys. Chem. Min.*, **15**, 191–.

[230] Yao, H. and W.Y. Ching (1994), "Optical Properties of β–C_3N_4 and its Pressure Dependence", *Phys. Rev. B*, **50**, 11231–11234.

[231] Yu, K.M., M.L. Cohen, E.E. Haller, W.L. Hansen, A.Y. Liu and I.C. Wu (1994), "Observation of Crystalline C_3N_4", *Phys. Rev. B*, **49**, 5034–5037.

[232] Zhang, Z.J., S. Fan and C.M. Lieber (1995), "Growth and Composition of Covalent Carbon Nitride Solids", *Appl. Phys. Lett.*, **66**, 3582–3584.

[233] Zhogolev, D.A., O.P. Bugaets and I.A. Marushko (1981), "Compounds Isoelectronic With Diamond as a Basis for the Creation of New Hard and Superhard Materials" *Inorg. Chem.*, **22**, 33–38.

Vita

I was born April 12, 1966 to Michael Philip Teter and Jaqueline Anne Teter of Austin, Texas. I was then raised in the Finger Lakes region of New York state where I was able to spend much of my time outside catching snakes, climbing cliffs, crossing ice flows, swimming across lakes, and flying sailplanes. To my parent's astonishment, I survived to adulthood.

I then spent many years doing this and that and having a really good time.

All of this changed in October of 1995 when I married Stuart Wheatley Overbey. We lived on a beautiful farm in Floyd County, Virginia and the following summer, our daughter Elora Shea was born. I returned to Virginia Tech to finish my undergraduate degree in Materials Engineering. To my surprise, I did quite well and was offered a chance to be a graduate student of Jerry Gibbs. During the early part of my graduate career, our son William Finley was born. Since then we have lived in Washington D.C. where I was a predoctoral associate at the Geophysical Lab and in Blacksburg, Virginia where I have been finishing up my Ph.D. in Materials Engineering Science. It has been a wonderful opportunity and a great time.

Let's see what happens next.